Draft version January 6, 2017

Preprint typeset using LaTeX style AASTeX6 v. 1.0

arXiv:1701.01422v1 [astro-ph.SR] 5 Jan 2017

THE EXTINCTION PROPERTIES OF AND DISTANCE TO THE HIGHLY REDDENED TYPE IA SUPERNOVA SN 2012CU

X. Huang,[1] Z. Raha,[1] G. Aldering,[2] P. Antilogus,[4] S. Bailey,[2] C. Baltay,[5] K. Barbary,[3] D. Baugh,[6] K. Boone,[2,3] S. Bongard,[4] C. Buton,[7] J. Chen,[6] N. Chotard,[7] Y. Copin,[7] P. Fagrelius,[2,3] H. K. Fakhouri,[2,3] U. Feindt,[16] D. Fouchez,[9] E. Gangler,[10] B. Hayden,[2] W. Hillebrandt,[15] A. G. Kim,[2] M. Kowalski,[8,11] P.-F. Leget,[10] S. Lombardo,[8] J. Nordin,[2,8] R. Pain,[4] E. Pecontal,[12] R. Pereira,[7] S. Perlmutter,[2,3] D. Rabinowitz,[5] M. Rigault,[8] D. Rubin,[2,13] K. Runge,[2] C. Saunders,[2,3] G. Smadja,[7] C. Sofiatti,[2,3] A. Stocker,[17] N. Suzuki,[2] S. Taubenberger,[15] C. Tao,[6,9] R. C. Thomas [14]

(The Nearby Supernova Factory)

[1]Department of Physics and Astronomy, University of San Francisco, San Francisco, CA 94117-1080

[2] Physics Division, Lawrence Berkeley National Laboratory, 1 Cyclotron Road, Berkeley, CA, 94720

[3] Department of Physics, University of California Berkeley, 366 LeConte Hall MC 7300, Berkeley, CA, 94720-7300

[4] Laboratoire de Physique Nucléaire et des Hautes Énergies, Université Pierre et Marie Curie Paris 6, Université Paris Diderot Paris 7, CNRS-IN2P3, 4 place Jussieu, 75252 Paris Cedex 05, France

[5] Department of Physics, Yale University, New Haven, CT, 06250-8121

[6] Tsinghua Center for Astrophysics, Tsinghua University, Beijing 100084, China

[7] Université de Lyon, F-69622, Lyon, France ; Université de Lyon 1, Villeurbanne ; CNRS/IN2P3, Institut de Physique Nucléaire de Lyon.

[8] Institut fur Physik, Humboldt-Universitat zu Berlin, Newtonstr. 15, 12489 Berlin

[9] Centre de Physique des Particules de Marseille, Aix-Marseille Université , CNRS/IN2P3, 163 avenue de Luminy -

Case 902 - 13288 Marseille Cedex 09, France

[10] Clermont Université, Université Blaise Pascal, CNRS/IN2P3, Laboratoire de Physique Corpusculaire, BP 10448, F-63000 Clermont-Ferrand, France

[11] DESY, D-15735 Zeuthen, Germany

[12] Centre de Recherche Astronomique de Lyon, Université Lyon 1, 9 Avenue Charles André, 69561 Saint Genis Laval Cedex, France

[13] Space Telescope Science Institute, 3700 San Martin Drive, Baltimore, MD 21218

[14] Computational Cosmology Center, Computational Research Division, Lawrence Berkeley National Laboratory, 1 Cyclotron Road MS 50B-4206, Berkeley, CA, 94720

[15] Max-Planck-Institut für Astrophysik, Karl-Schwarzschild-Str. 1, D-85748 Garching, Germany

[16] The Oskar Klein Centre, Department of Physics, AlbaNova, Stockholm University, SE-106 91 Stockholm, Sweden

[17] Department of Mathematics, University of Colorado, Campus Box 395, Boulder, Colorado 80309-0395

ABSTRACT

Correction of Type Ia Supernova brightnesses for extinction by dust has proven to be a vexing problem. Here we study the dust foreground to the highly reddened SN 2012cu, which is projected onto a dust lane in the galaxy NGC 4772. The analysis is based on multi-epoch, spectrophotometric observations spanning 3,300 - 9,200 Å, obtained by the Nearby Supernova Factory. Phase-matched comparison of the spectroscopically twinned SN 2012cu and SN 2011fe across 10 epochs results in the best-fit color excess of ($E(B-V)$, RMS) = $(1.00, 0.03)$ and total-to-selective extinction ratio of (R_V, RMS) = $(2.95, 0.08)$ toward SN 2012cu within its host galaxy. We further identify several diffuse interstellar bands, and compare the 5780 Å band with the dust-to-band ratio for the Milky Way. Overall, we find the foreground dust-extinction properties for SN 2012cu to be consistent with those of the Milky Way. Furthermore we find no evidence for

significant time variation in any of these extinction tracers. We also compare the dust extinction curve models of Cardelli et al. (1989), O'Donnell (1994), and Fitzpatrick (1999), and find the predictions of Fitzpatrick (1999) fit SN 2012cu the best. Finally, the distance to NGC4772, the host of SN 2012cu, at a redshift of $z = 0.0035$, often assigned to the Virgo Southern Extension, is determined to be 16.6±1.1 Mpc. We compare this result with distance measurements in the literature.

1. INTRODUCTION

The distance measurements of Type Ia supernovae (SNe Ia) led to the discovery of the accelerated expansion of the universe (Riess et al. 1998; Perlmutter et al. 1999). This technique, based on the standardizability of the peak luminosity of SNe Ia, remains one of the most powerful probes to understand the cause of the acceleration (e.g., Suzuki et al. 2012; Betoule et al. 2014; Rest et al. 2014). This is especially true in light of recent developments in standardization techniques that promise to substantially reduce brightness dispersion from the canonical value of ~ 0.15 mag, alternatively based on the incorporation of near-IR light curves, Si II λ6355 Å absorption line velocity, and local star formation rate (Mandel et al. 2011; Barone-Nugent et al. 2012; Wang et al. 2009; Foley & Kasen 2011; Rigault et al. 2013; Kelly et al. 2015). Recently, Fakhouri et al. (2015) proposed a new standardization procedure based on a spectroscopic twinning method in the optical range that produces a dispersion that is as good as the best of the other standardization methods. With the prospect that the variation due to the astrophysical differences of SNe Ia can be further minimized with the twinning method, dust remains one of the last key sources of systematic uncertainty.

Following Cardelli et al. (1989), dust extinction properties are often characterized by one parameter, $R_V \equiv A_V/E(B-V)$, the total-to-selective extinction ratio. The interstellar dust in the Milky Way (MW) has a well-known average R_V of 3.1 (e.g., Draine 2003; Schlafly & Finkbeiner 2011). The

slope of the color standardization for SNe Ia is determined by minimizing the rest-frame B-band luminosity (M_B) scatter (e.g. Tripp 1998; Tripp & Branch 1999). The slope, usually denoted as β (e.g., Guy et al. 2010, Equation 5), could naively be expected to equal R_B ($= R_V + 1$), but likely mixes the effects of SN intrinsic color variation and dust. In fact, typical fits for β yield much lower values (e.g., Tripp 1998; Hicken et al. 2009; Wang et al. 2009) than expected given the MW average R_V.

Chotard et al. (2011) shed light on this apparent discrepancy. Exploiting the fact that spectral features are independent of dust extinction, they first showed that by applying corrections based on the equivalent widths (EW's) of Si II λ4131 Å and Ca II H&K features, two highly variable regions in the SN spectra, the mean empirical extinction law obtained by minimizing M_B scatter for their SN sample became much smoother and conformed well to the extinction law of Cardelli et al. (1989, CCM89). Secondly, by adopting a color covariance matrix that is different from the one based on the output of the SALT2 lightcurve fitter(Guy et al. 2007), they obtained $R_V = 2.8 \pm 0.3$, in agreement with the average MW value. It remains the case, however, that many highly reddened SNe tend to have R_V lower than 2 (e.g., Mandel et al. 2011; Phillips et al. 2013). A recent example is SN 2014J, a well-observed, highly reddened SN Ia with a R_V of 1.4 – 1.7 and $E(B-V)$ of 1.2 – 1.4 (Goobar et al. 2014; Amanullah et al. 2014; Foley et al. 2014; Marion et al. 2015; Brown et al. 2015). These results are not derived from brightness-color behavior, as with the β parameter mentioned above, but rather are obtained from a fit to the shape of the SN spectral energy distribution (SED) using an extinction curve parametrized by R_V.

Unlike for cosmological studies, in order to understand the extinction properties of host galaxies, highly reddened SNe are useful. Comparing a reddened SN Ia with its spectroscopic twin that is little affected by dust would allow the study of host-galaxy extinction without the confusion of intrinsic color variation. SN 2012cu presents such an opportunity, as it has one of the highest extinction

values observed to date. Furthermore, SN 2011fe, in many regards the best studied SN Ia, is a spectroscopic twin of SN 2012cu. The fact that SN 2011fe has little or no dust (Nugent et al. 2011) is also quite important, since comparison to SN 2012cu will provide the total — not just differential — extinction. In this paper, with SN 2011fe as the template, we analyze the wavelength-dependent extinction of SN 2012cu using a spectrophotometric time series obtained by the Nearby Supernova Factory (SNfactory, Aldering et al. 2002). While the nearly ideal pairing between SN 2012cu and SN 2011fe perhaps is rare today, such samples should continue to grow. The R_V distribution found nearby will then inform high-redshift studies, just as lightcurve parameters now do.

With SN 2012cu de-reddened, we further demonstrate that in the case of SN 2012cu and SN 2011fe the twinning approach can provide highly precise and accurate relative distance measurements, as Fakhouri et al. (2015) found.

This paper is organized as follows. We present our spectroscopic observations of SN 2012cu in § 2. In § 3, we measure $E(B-V)$, R_V, A_V, and the relative distance between SN 2012cu and SN 2011fe, using data from 10 epochs between -6.8 and 23.2 days measured relative to the DayMax parameter of the SALT lightcurve fitter (Guy et al. 2007, 2010). We explore different approaches for handling spectral mismatches that remain. We also measure the EWs of Na I and a diffuse interstellar band (DIB) feature at 5780 Å and examine whether these feature exhibit time variability. In § 4, we determine the distance to the host galaxy of SN 2012cu and discuss the nature of foreground dust in its host. We present our conclusions in § 5.

2. OBSERVATIONS

SN 2012cu was discovered on 2012, June 11.2 UT (Itagaki et al. 2012; Ganeshalingam et al. 2012) and was classified as a Type Ia on 2012, June 15 UT (Marion et al. 2012; Zhang et al. 2012). NGC 4772 is the host, at a heliocentric redshift of $z = 0.003469 \pm 0.000017$ (de Vaucouleurs et al. 1991).

Figure 1 shows our V-band image of SN 2012cu and the host galaxy, NGC 4772. The upper left inset is an image from the Wide-Field Infrared Survey Explorer (WISE, Wright et al. 2010) in the 12-μm band, which spans the wavelengths of some of the emission features of polycyclic aromatic hydrocarbons (PAHs) associated with dust (Li & Draine 2001). The upper right inset is a GALEX (Bianchi et al. 2014) image that highlights the young stars along the dust lane. The comparison of these images shows that SN 2012cu is projected onto a dust ring. There is a reasonably high probability that SN 2012cu is behind or embedded in the dust lane, and that it is mostly reddened by this dust detected in the interstellar medium (ISM) of the host galaxy.

Spectra of SN 2012cu, spanning 17 epochs from -6.8 to 46.2 days. were obtained by the SNfactory collaboration with its SuperNova Integral Field Spectrograph (SNIFS, Aldering et al. 2002; Lantz et al. 2004) on the University of Hawaii 2.2-m telescope on Mauna Kea. For the wavelength range of 3,300 - 9,200 Å, the spectra of SN 2012cu are flux calibrated (Buton et al. 2013), host-galaxy subtracted (Bongard et al. 2011), corrected for Milky Way extinction (Schlafly & Finkbeiner 2011), and then de-redshifted to the rest frame for subsequent analysis. Further details, including the observing log, a figure showing the entire the spectral time series, and information on how to access these data are provided in Appendix B.

[1] http://ned.ipac.caltech.edu/

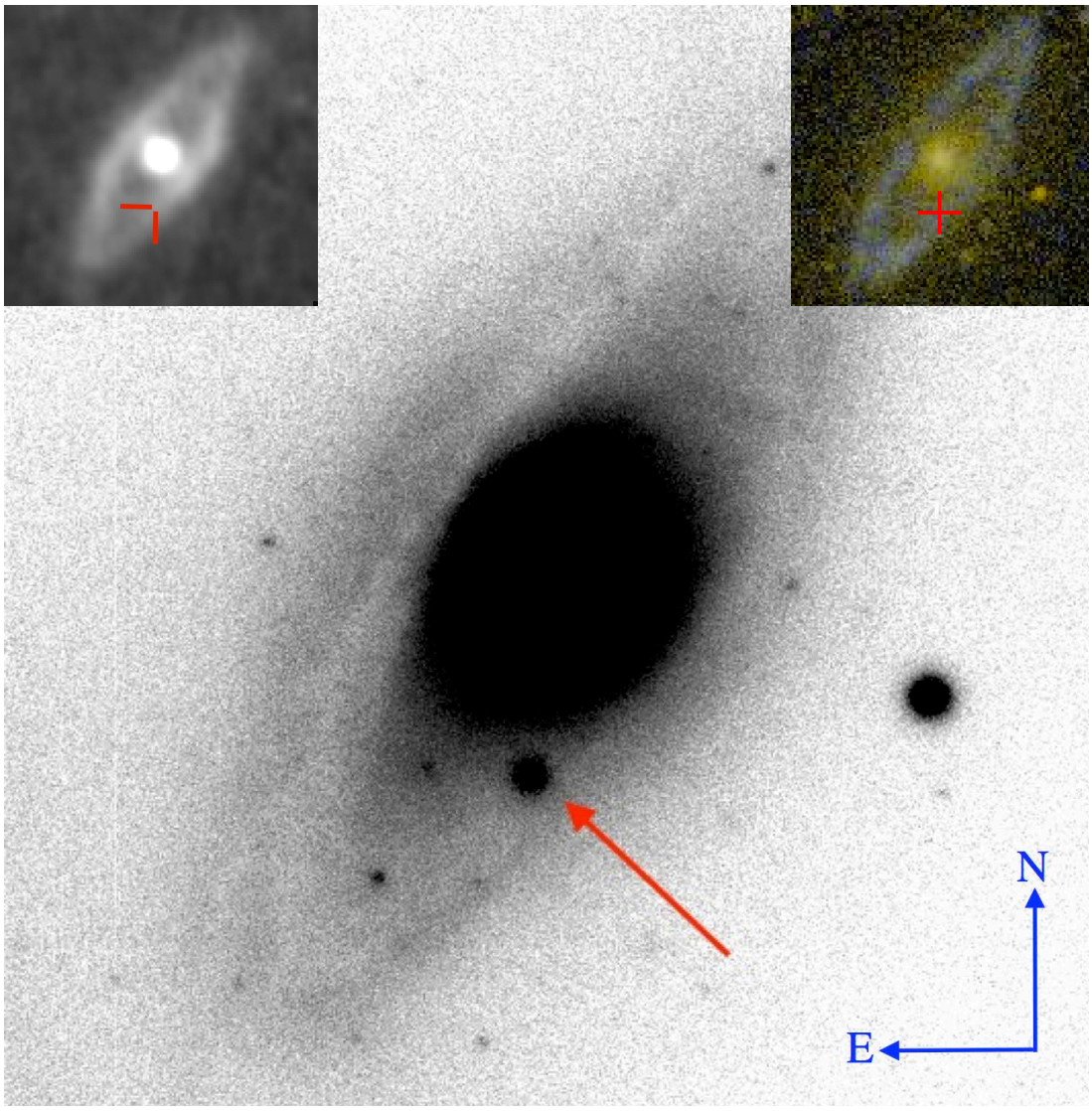

Figure 1. V-band image of SN 2012cu (arrow) acquired using SNIFS. The compass arrows are 20″ long. The inset at the upper left is the WISE 12-μm image of the host galaxy NGC 4772, with the approximate projected position of SN 2012cu marked. Both images clearly show the presence of a dust ring, in absorption in V-band and in emission at 12 μm. The inset at the upper right is the GALEX image that shows the young stars along the dust lane in NGC 4772, with the crosshairs marking the position of SN 2012cu.

3. DUST EXTINCTION PROPERTIES

In this section, we first describe how we fit for the dust extinction curve and the distance modulus difference ($\Delta\mu$) between SN 2012cu and SN 2011fe (§ 3.1). In this effort, we explore different de-weighting schemes for regions where spectral differences are present. We then turn our attention to

Na I and diffuse interstellar band (DIB) features in the SN 2012cu spectra (§ 3.2). Dust extinction curves are parametrized by quantities denoted as $E(B-V)$ and R_V; these are not required to match the values that would be measured only using the B and V bands.

3.1. *Extinction Curve and Distance Modulus Difference*

3.1.1. *Simultaneously Fitting for $E(B-V)$, R_V and $\Delta\mu$*

The best-fit SALT2.4 parameters for SN 2012cu are first determined to be $(x_1', c') = (0.021 \pm 0.123, 0.971 \pm 0.030)$ and DayMax$'$ = MJD 56104.89 $\pm$ 0.15. Given the extreme color of SN 2012cu, much higher than the typical reddening in the training data for SALT, we apply an initial de-reddening using the extinction curve of Fitzpatrick (1999) and perform the fit again. We find $x_1 = -0.269 \pm 0.078$ and DayMax = MJD 56105.06 $\pm$ 0.11. The DayMax value has shifted by +0.16 days, and corresponds to June 27.1 UT. To be consistent, we perform the SALT2.4 fit for SN 2011fe as well, and obtain $(x_1, c) = (-0.280 \pm 0.093, -0.058 \pm 0.027)$ and DayMax = 55815.20 $\pm$ 0.08. (Our x_1, c, and DayMax are in good agreement with the corresponding values in Pereira et al. (2013), using SALT2.2.) The x_1 parameter is now very similar for these two SNe. We further determine that this pair has a near-maximum twinness ranking = 0.1, on a scale from 0 to 1, placing the pairing of these two SNe among the best spectroscopic "twins" (Fakhouri et al. 2015, Figure 5). It is even the case that both SNe exhibit the rare C II feature (Thomas et al. 2011), albeit at higher velocity for SN 2012cu at the earliest phase, strengthening the case for the similarity of the explosion physics.

As SN 2011fe suffers nearly no host extinction, for the rest of this paper we treat its spectra, which have been corrected for mild Milky Way (MW) extinction ($E(B-V) = 0.0088$ mag) by Pereira et al. (2013), as if they were un-reddened versions of SN 2012cu spectra.

To determine the effects of dust reddening for SN 2012cu, we first pair the SN 2011fe spectra, also obtained with SNIFS (Pereira et al. 2013), with those of SN 2012cu for cases where the phase

difference is less than one day. This is possible for 10 SN 2012cu phases between −6.8 and 23.2 days, thanks to the dense temporal sampling of the Pereira et al. (2013) data set (see Table 1). In this paper, the phases for both SNe are always measured relative to their respective DayMax. The phase differences (0.2 – 0.3 days; see Table 1) are somewhat larger than the combined phase uncertainty between the two SNe (0.14 days). As a test, we have performed interpolation for several phases, including for phase pairings with a 0.3 d phase difference, and find these phase differences make very little difference for the best-fit results. Thus there is no need to interpolate.

For these 10 pairs of spectra, we divide the fluxes evenly into 925 bins above 3600 Å; between 3300 Å and 3600 Å we use two bins due to the lower S/N here for the highly reddened SN 2012cu. Therefore there are a total of 927 bins. We use these same bins for both SNe.

The extinction curve models of Cardelli et al. (1989), O'Donnell (1994), and Fitzpatrick (1999) (CCM89, OD94, and F99, respectively) are the most commonly used in the literature. All three are parameterized by R_V and $E(B-V)$. F99 pointed out the tension between observation and CCM89 in the wavelength range that roughly corresponds to the i and r bands. This has been subsequently confirmed by other authors, not just for CCM89 but also for OD94 (e.g. Schlafly et al. 2010; Mörtsell 2013). A more detailed discussion is given in Appendix A. For the remainder of this section, we will use F99.

As we will show below, despite being good "twins", the high S/N ratio of the SNIFS data makes the differences in spectral features between SN 2011fe and SN 2012cu clearly visible. Such differences are stronger for pre-maximum phases. We compare three approaches toward the regions where the spectral differences are high. In Approach I, we will treat all wavelength bins in the same manner. In Approach II, we will identify and de-weight these regions appropriately. Finally in Approach III, we will discard these regions altogether in the fitting process.

Table 1. Phase Comparison and Best-Fit Parameters Using Approach I

Pair ID	SN 2012cu	SN 2011fe	$E(B-V)$	R_V	$\Delta\mu$	A_V	χ^2_ν
	Phase (days)	Phase (days)				$(= R_V \cdot E(B-V))$	
1	−6.8	−7.0	0.995 ± 0.005	2.908 ± 0.024	1.964 ± 0.013	2.895 ± 0.015	51.22
2	−1.7	−2.0	0.989 ± 0.006	3.082 ± 0.025	1.873 ± 0.012	3.048 ± 0.014	88.48
3	3.3	3.0	1.019 ± 0.006	2.987 ± 0.024	1.868 ± 0.012	3.043 ± 0.013	99.05
4	6.3	6.0	1.017 ± 0.006	2.962 ± 0.023	1.864 ± 0.011	3.012 ± 0.013	53.41
5	8.3	8.0	1.010 ± 0.007	2.970 ± 0.024	1.884 ± 0.011	3.001 ± 0.012	22.70
6	11.2	11.0	0.982 ± 0.006	2.992 ± 0.024	2.043 ± 0.010	2.939 ± 0.012	20.49
7	16.2	16.0	0.911 ± 0.008	3.218 ± 0.033	2.016 ± 0.011	2.931 ± 0.013	27.47
8	18.2	18.0	0.907 ± 0.009	3.270 ± 0.038	1.968 ± 0.013	2.966 ± 0.015	57.26
9	21.2	21.0	0.912 ± 0.011	3.265 ± 0.041	2.027 ± 0.012	2.976 ± 0.014	53.03
10	23.2	23.0	0.915 ± 0.011	3.177 ± 0.041	1.998 ± 0.012	2.908 ± 0.014	26.77

For Approach I, when we simultaneously fit for $E(B-V)$, R_V, and $\Delta\mu$, only measurement uncertainties are included. For each phase the fit must de-redden the spectrum of SN 2012cu using the dust extinction curve of F99, calculate the AB magnitude (see, e.g., Bessell & Murphy 2012) for each bin, $m_{AB,k}^{\rm 12cu,\,dereddened}(E(B-V), R_V)$, which can be more conveniently written as $m_{AB,k}^{\rm 12cu} + 2.5\log(F99(E(B-V), R_V))$, and then compare the results with SN 2011fe. For each separate

matching phase, we therefore minimize

$$\chi^2 = \sum_k \frac{\left[m^{\rm 12cu}_{AB,\,k} - m^{\rm 11fe}_{AB,\,k} + 2.5\log(F99(E(B-V), R_V)) - \Delta\mu\right]^2}{\sigma^2_{k,\rm meas}}, \quad (1)$$

where $\sigma^2_{k,\rm meas} = \left(\sigma^{\rm 11fe}_{AB,\,k}\right)^2 + \left(\sigma^{\rm 12cu}_{AB,\,k}\right)^2$ is the total measurement variance for bin k in magnitude space. SN 2012cu has a wavelength-independent ("gray") scatter of 0.025 mag, uncorrelated between phases (Buton et al. 2013). For SN 2011fe it is between 0.03 – 0.06 mag, again uncorrelated between phases. These larger values stem from the unusually high airmasses at which some SN 2011fe observations were taken. Effectively this gray scatter is absorbed into the uncertainty for $\Delta\mu$ and does not affect χ^2.

In Figure 2 we show the binned spectrum of SN 2012cu at phase −6.8 days in units of AB magnitude, dereddened with the best-fit $E(B-V)$ and R_V and vertically shifted by the best-fit $\Delta\mu$, together with the spectrum of SN 2011fe for the corresponding phase. The minimum reduced χ^2 is $\chi^2_\nu = 51.22$. It is evident that this high value of χ^2_ν is due to spectral feature differences between the two SNe. In the next section, we will present our main approach to address the unaccounted-for uncertainty. Here, to set a baseline for comparison with Approaches II and III, we simply uniformly inflate the errors so that χ^2_ν is rescaled to 1. This does not change best-fit values or the shape of confidence contours. The error bars on the fitting parameters in the top panel are those computed after this rescaling. The vertical green bands are the regions of the highly variable Si II and Ca II features identified in Chotard et al. (2011), which will be henceforth referred to as the "Chotard regions." Outside of these regions, some of the other well-known SN spectral features are also labeled. The sharp feature around 5896 Å labeled in red is Na I D absorption. The bottom panel shows the residual of the fit weighted by the measurement uncertainties, or the "pull spectrum." It is clear that the two spectra can be very different outside of the Chotard regions, as well. As examples (see Figure 2), they are

significantly different for: (i) the regions of Fe II $\lambda\lambda$5018, 5169, S II λ5640, and O I λ7773, (ii) the emission part of the P-Cygni profile of one of the Chotard Si II features, centered around 6350 Å, and (iii) the emission part of the Ca II IR triplet, centered around 8600 Å.

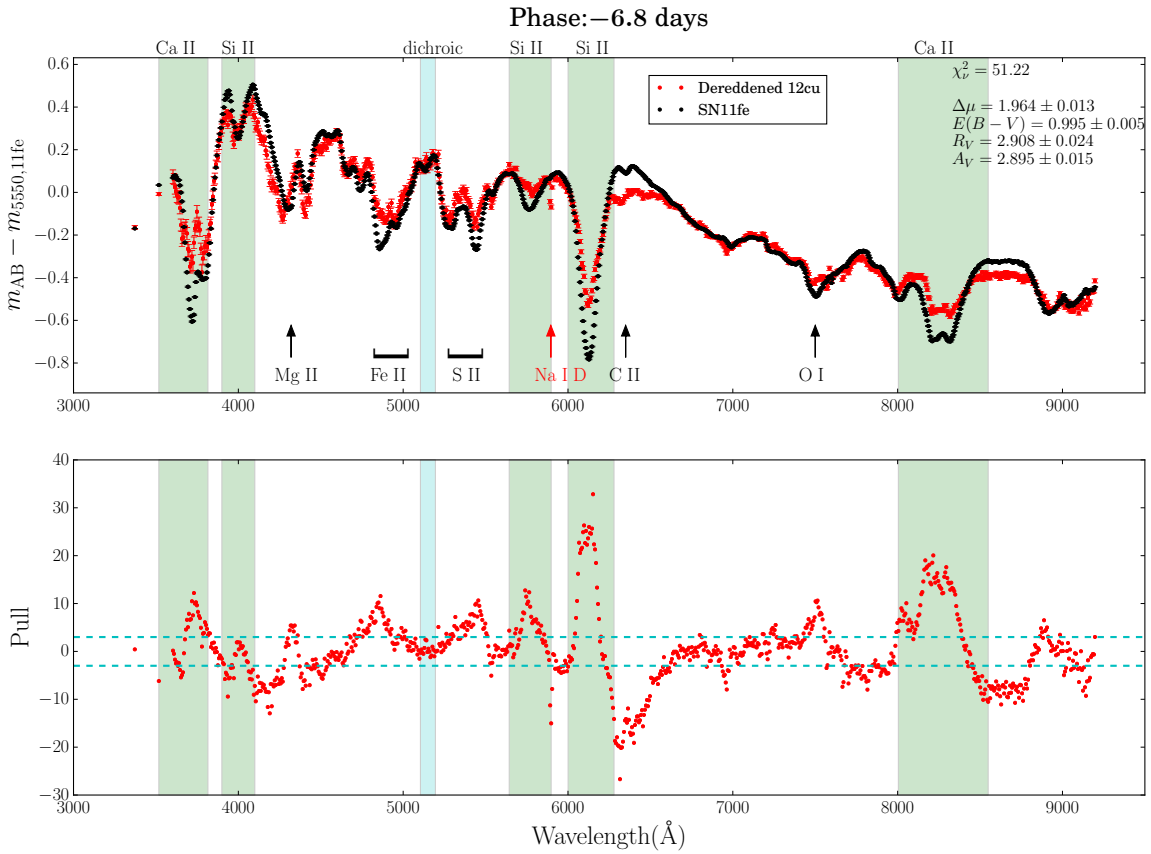

Figure 2. **Top Panel** shows the binned SN 2012cu spectrum (red) in units of AB magnitude for the phase of −6.8 days dereddened with the best-fit $E(B-V)$ and R_V, and shifted vertically by the best-fit $\Delta\mu$, for comparison with the template spectrum of SN 2011fe (black) for the same phase. The zero point is arbitrary, chosen to be the magnitude at 5550 Å for SN 2011fe. Even for well-twinned SNe, it is for pre-maximum phases that spectral differences are more likely, so this pair is among those with the largest level of disagreement. Very small differences can be seen here given the high S/N ratio of these spectra. For comparison at later phases, see Figure 4. The vertical green bands are the regions of the Si II and Ca II features found to be highly variable between SNe in Chotard et al. (2011). Outside of these regions, some of the other well-known SN spectral features are also labeled, as well as the Na I D absorption feature. **Bottom Panel** shows the difference in magnitude between the two spectra in the top panel (the residual), weighted by measurement uncertainty, or the "pull." The peaks and valleys correspond to where the spectra are the most different. The cyan dashed lines indicate $3\,\sigma$ deviation. It is clear that the high value of χ^2_ν is due to spectral feature differences between the two SNe, despite the fact that they are good matches relative to other SNe. While the Chotard regions capture the greatest spectral variations, the two spectra can nonetheless be very different outside of these regions.

In Figure 3, we present the confidence contours for $E(B-V)$ and R_V, after rescaling χ^2_ν to 1, which is equivalent to inflating the variances in Equation 1 uniformly across all wavelengths, and marginalizing over the distance modulus difference $\Delta\mu$. $E(B-V)$ and R_V are clearly anti-correlated; this is true for all 10 phases. The uncertainties for the extinction, A_V (simply the product of the best-fit $E(B-V)$ and R_V), are computed by taking into account the covariance between these two quantities. It is notable that, owing to this anti-correlation, the uncertainty for A_V is smaller than for R_V.

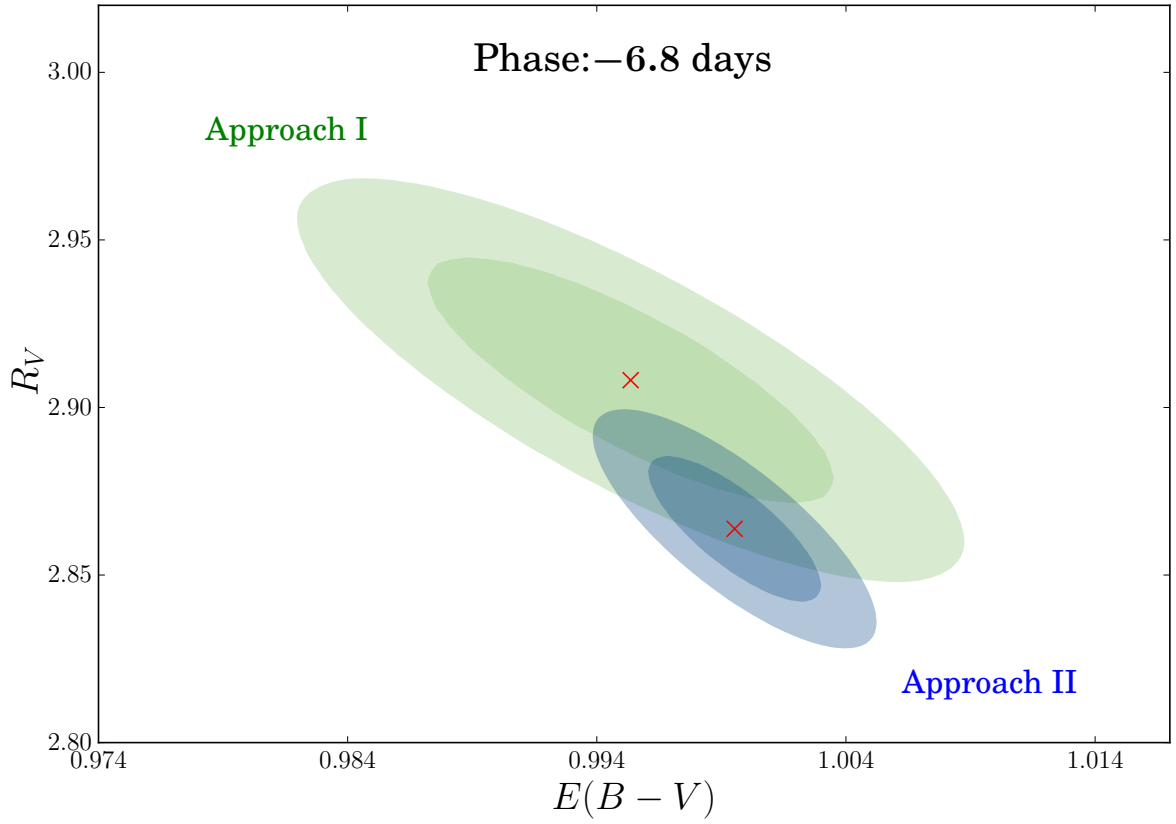

Figure 3. The green contours indicate the 1 and 2 σ confidence regions for $E(B-V)$ and R_V for the phase of −6.8 days for Approach I (see text). The cross marks the best-fit values. Likewise, the blue contours are for Approach II. All 10 phases between −6.8 and 23.2 days exhibit a similar anti-correlation between these two fitting parameters.

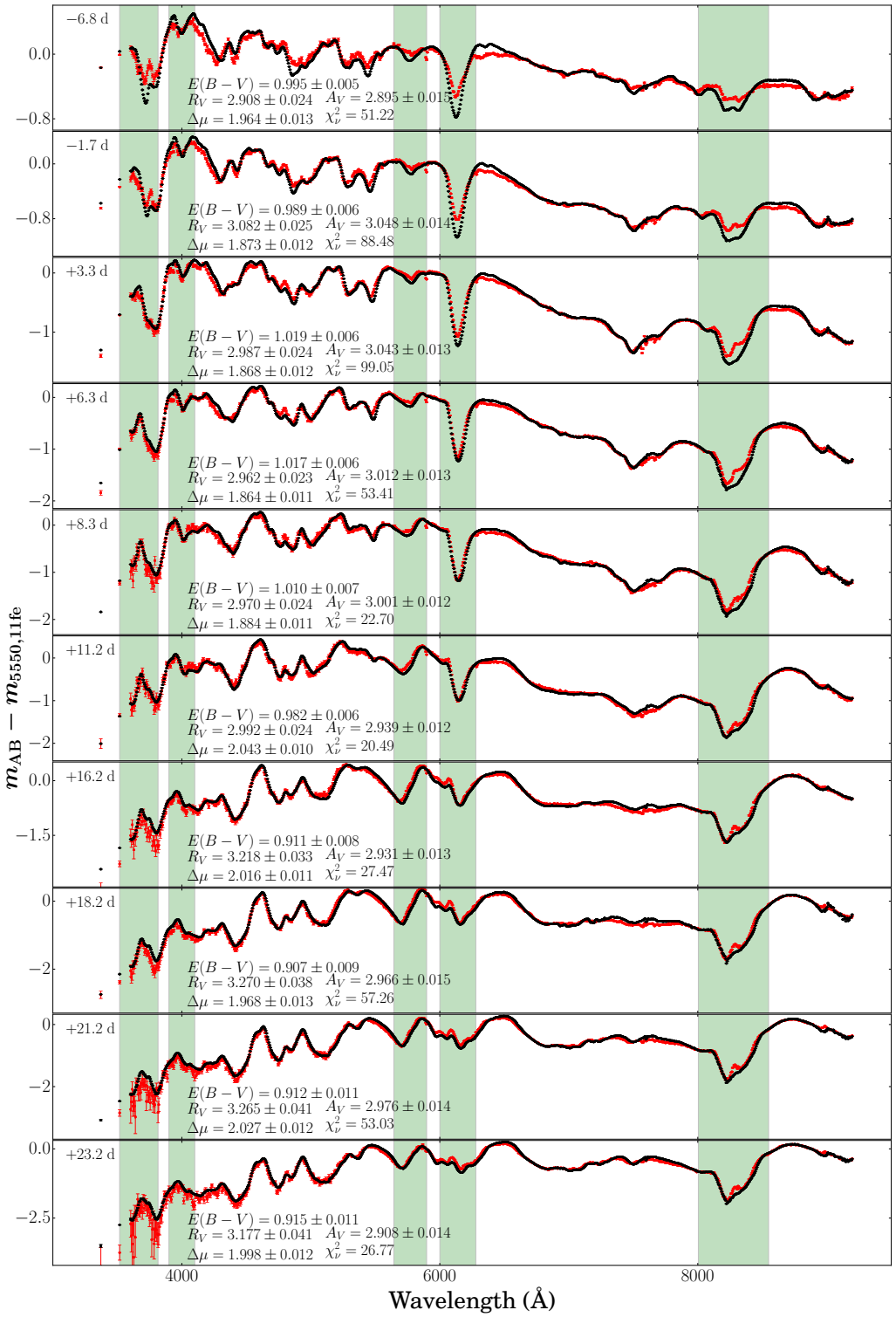

Figure 4. Full SN 2012cu spectrophotometric time series used in the analysis. The phases are shown in the upper left corner of each panel. Binned SN 2012cu spectra (red) in units of AB magnitude dereddened with the best-fit $E(B-V)$ and R_V, and shifted vertically by the best-fit $\Delta\mu$, are shown together with spectra of SN 2011fe with corresponding phases. As with Figure 2, the vertical green bands are the Chotard regions.

We apply the same fitting procedure to each of the 10 phases. The results are shown in Figure 4. Larger values of χ^2_ν are, generally, associated with the earlier phases, owing to their greater spectral diversity. We will address this issue further in the next subsection, §3.1.2. The phase-by-phase summary for the best-fit $E(B-V)$, R_V, $\Delta\mu$, and the derived quantity, A_V, are presented in Table 1. The uncertainty-weighted average and RMS values across the ten phases (Table 1), are ($E(B-V)$, RMS) = (0.983, 0.046) mag, (R_V, RMS) = (3.035, 0.131), ($\Delta\mu$, RMS) = (1.952, 0.068) mag, and (A_V, RMS) = (2.973, 0.051) mag. Conservatively, for R_V and $E(B-V)$, we take the uncertainties on the means to be the RMS dispersions. The uncertainty on $\Delta\mu$ is discussed in § 4.1, as it requires further consideration.

3.1.2. *Effects of Spectral Feature Differences*

In the previous section we showed that even though SN 2012cu and SN 2011fe are good "twins," there are significant spectral differences between them. In this section, by presenting the results of two alternative ways to handle these spectral feature differences, we will show that they do *not* have a significant effect on the best-fit extinction and relative distance parameters.

In Approach II, we de-weight SN spectral feature differences but leave differences due to measurement noise intact. To identify where the spectra behave differently for SN 2011fe and SN 2012cu the terms in the summation in Equation 1 are plotted against the central wavelengths of the corresponding bins. As shown in Figure 2, in the $(residual/\sigma)$ spectrum, or pull spectrum, the locations of the peaks and valleys are where the spectra of 2011fe and 2012cu are most different. We convolve the pull spectrum with a Gaussian kernel and through trial and error find that a Gaussian with a standard deviation of 25 Å captures the spectrally correlated differences (features) discernible by eye (Figure 5). We now use the result of the convolution, p_k, to de-weight the spectral differences. First

we set p_k to zero for the wavelength bins where $|p_k| \leq 3$. We de-weight the complementary bins, where $|p_k| > 3$, by rescaling p_k in such a way that when added in quadrature to the denominator in Equation 1 the reduced χ^2 for these regions is 1. The spectral regions that are not de-weighted span the full wavelength range. We then add the rescaled p_k^2 to $\sigma_{k,\mathrm{meas}}^2$ in the denominator of Equation 1. In order to achieve an average $\chi_\nu^2 \sim 1$ across all phases, we find that for the wavelength regions where $|p_k| \leq 3$, it is necessary to add an error floor of $\sigma_{\mathrm{floor}} = 0.03$ mag. This error floor is treated as an uncorrelated error, and is not related to the gray scatter mentioned in §3.1.1. Thus Equation 1 becomes

$$\chi^2 = \sum_k \frac{\left[m_{AB,k}^{12\mathrm{cu}} - m_{AB,k}^{11\mathrm{fe}} + 2.5\log(F99(E(B-V), R_V)) + \Delta\mu\right]^2}{\sigma_{k,\mathrm{meas}}^2 + p_k^2 + \sigma_{\mathrm{floor}}^2}. \quad (2)$$

Using Equation 2, we once more perform χ^2 minimization. In Figure 5 we show the best-fit de-reddened SN 2012cu spectrum at -6.8 days, vertically shifted by the best-fit $\Delta\mu$, together with the 2011fe spectrum at the corresponding phase. We obtain $\chi_\nu^2 = 0.90$, close to 1 as expected. We note the pull values (third panel in Figure 5) for $\lambda \lesssim 6000$ Å are slightly larger than for the longer wavelengths because the measurement uncertainties for the bluer wavelengths are larger due to extinction and therefore a uniform error floor doesn't have as much of an effect. However, we will show below that the particular choice of weighting scheme doesn't affect the best-fit results in a significant way. We then apply the same fitting procedure to each of the 10 phases. The results are presented in the left panels of Figure 6 and Table 2. The values of χ_ν^2 now range from 0.78 to 1.24. The right panels of Figure 6 show the convolution result for the pull spectrum for each of the 10 epochs.

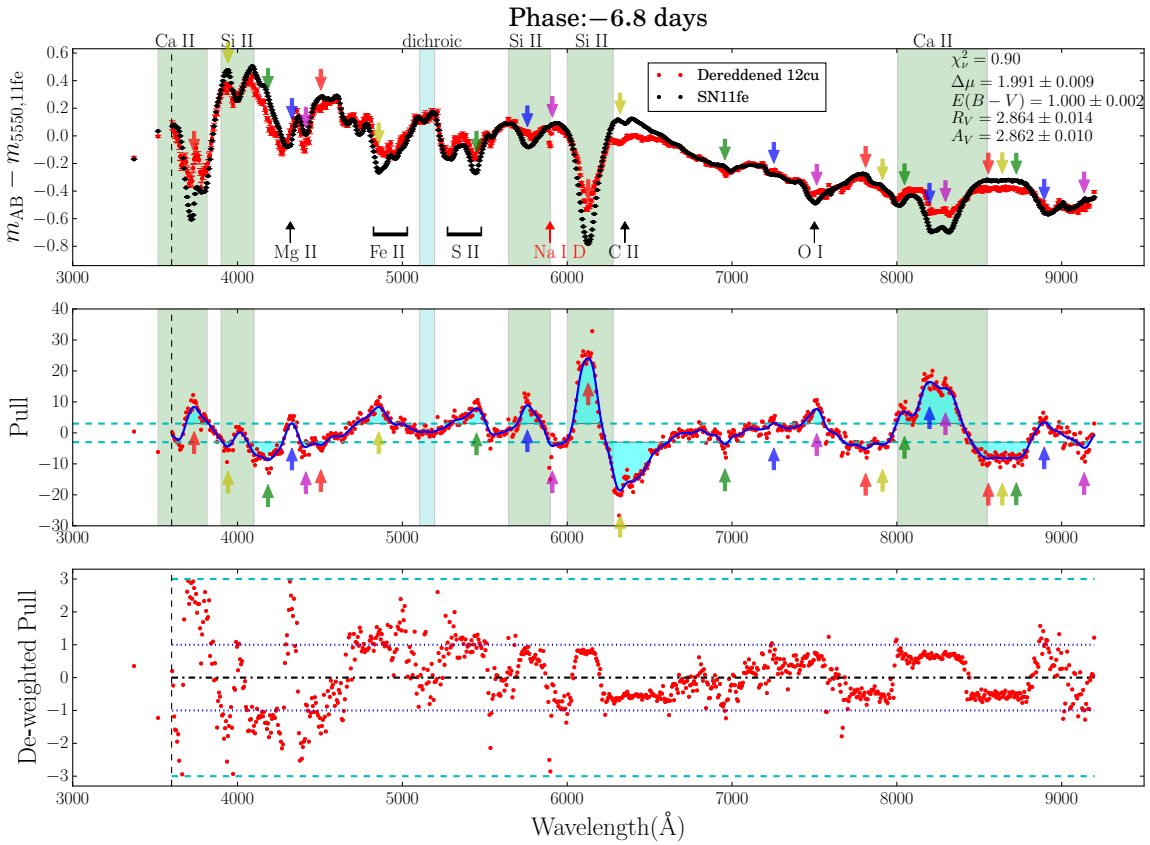

Figure 5. This figure demonstrates the technique used in Approach II, to de-weight the regions where the spectral differences between SN 2011fe and SN2012cu are large. **Top Panel**: The best-fit result after our technique has been applied, achieving $\chi^2_\nu \sim 1$ as expected. **Middle Panel**: This panel demonstrates the de-weighting used in this technique. The pull spectrum shown here is the same as the one in the middle panel of Figure 2, i.e., before de-weighting. The solid blue line is the result of the Gaussian convolution (see text). Each arrow points to an extremum whose absolute value is greater than $3\,\sigma$, marked by the cyan dashed lines. The arrows are matched by color between the top and middle panels and demonstrate that spectral feature differences are identified by this technique. The filled cyan regions are the wavelength regions where the deviation is greater than $3\,\sigma$. To de-weight these regions, an appropriately scaled quantity, p_k (see text), is added in quadrature to the measurement uncertainty in Equation 1 so that the χ^2_ν for these cyan regions is 1. In addition we add a 0.03 mag error floor to the complementary wavelength regions, where the deviation $\leq 3\,\sigma$, to achieve an average $\chi^2_\nu \sim 1$ across all phases (see Top Panel). **Bottom Panel**: The pull spectrum after the application of our technique (i.e., after de-weighting). The blue dotted and cyan dashed lines indicate 1 and $3\,\sigma$ deviations, respectively.

The weighted average and RMS values across the 10 phases are ($E(B-V)$, RMS) = $(1.002, 0.031)$, (R_V, RMS) = $(2.952, 0.081)$, ($\Delta\mu$, RMS) = $(1.982, 0.061)$, and (A_V, RMS) = $(2.944, 0.043)$. These results, along with those from Approach I, are summarized in Table 3 and Figure 7. Once again we take the uncertainties on the means for R_V and $E(B-V)$ to be the RMS dispersions across phases.

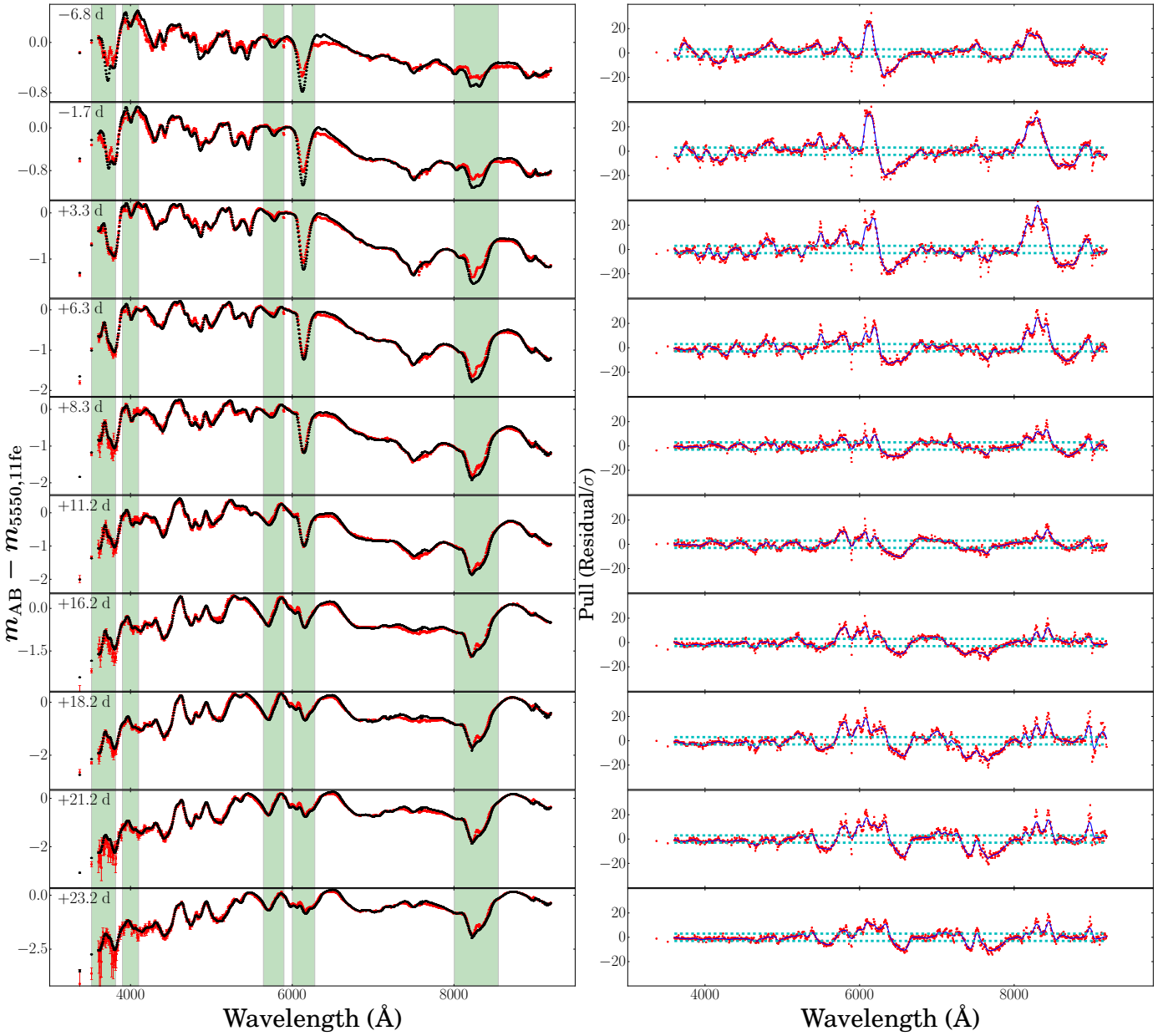

Figure 6. The left panels are the same as Figure 4, except the fitting process now is that of Approach II, which de-weights the wavelength regions where there are significant spectral feature differences (see text). The results of convolving the pull spectrum for each phase with a Gaussian kernel are shown in the right panels. The cyan dashed lines indicate $3\,\sigma$ deviations.

We have pursued one more approach. In Approach III, we increase p_k to an arbitrarily high value, essentially removing data in the wavelength regions with pull values greater than 3 (the cyan regions in Figure 5) from the fitting process. The average values of our best-fit parameters across

the 10 epochs are ($E(B-V)$, RMS) = (0.999, 0.029), (R_V, RMS) = (2.963, 0.079), ($\Delta\mu$, RMS) = (1.972, 0.067), and (A_V, RMS) = (2.950, 0.048). These results are very close to those obtained in Approach II. The agreement among the results from these three approaches — to well within their RMS fluctuations (Table 3) — shows that our best-fit results are not sensitive to the particular scheme of de-weighting the regions of high spectral variation, including simply uniformly increasing the measurement uncertainties with no relative de-weighting (Approach I). However, the RMS values improve substantially when some reasonable form of de-weighting is applied to spectral features.

Table 2. Spectral Features De-weighted Best-Fit Parameters Using Approach II

SN 2012cu	$E(B-V)$	R_V	$\Delta\mu$	A_V	χ^2_ν
Phase (days)				$(= R_V \cdot E(B-V))$	
−6.8	1.000 ± 0.002	2.864 ± 0.014	1.991 ± 0.009	2.862 ± 0.010	0.90
−1.7	0.998 ± 0.002	3.012 ± 0.014	1.912 ± 0.009	3.006 ± 0.010	0.83
3.3	1.038 ± 0.002	2.886 ± 0.013	1.918 ± 0.008	2.995 ± 0.009	0.77
6.3	1.033 ± 0.002	2.871 ± 0.014	1.909 ± 0.009	2.967 ± 0.010	0.88
8.3	1.019 ± 0.003	2.917 ± 0.017	1.913 ± 0.010	2.972 ± 0.011	1.22
11.2	0.987 ± 0.003	2.953 ± 0.018	2.063 ± 0.009	2.915 ± 0.011	1.24
16.2	0.947 ± 0.003	3.081 ± 0.020	2.038 ± 0.009	2.917 ± 0.011	1.20
18.2	0.953 ± 0.003	3.078 ± 0.020	2.008 ± 0.010	2.933 ± 0.011	1.02
21.2	0.966 ± 0.004	3.063 ± 0.019	2.058 ± 0.009	2.958 ± 0.010	0.99
23.2	0.967 ± 0.004	2.992 ± 0.020	2.027 ± 0.009	2.893 ± 0.011	1.17

The average values for the fitting parameters determined by Approach II in this subsection (§3.1.2) are adopted as the best-fit host galaxy reddening ($E(B-V)$) and total-to-selective extinction ratio (R_V), and distance modulus difference between SN 2012cu and SN 2011fe ($\Delta\mu$). This approach gives the lowest RMS on A_V and $\Delta\mu$. Our best-fit $E(B-V)$ $(= 1.00 \pm 0.03)$ compares well with the value $E(B-V) = 0.99 \pm 0.03$ reported by Amanullah et al. (2015) based on broadband photometry from

UV to NIR for SN 2012cu using the extinction curve of F99. Our best-fit R_V ($= 2.95 \pm 0.08$) is slightly higher than their $R_V = 2.8 \pm 0.1$. It is striking that optical spectrophotometry alone performs as well as combined UV, optical, NIR broadband photometry for this case.

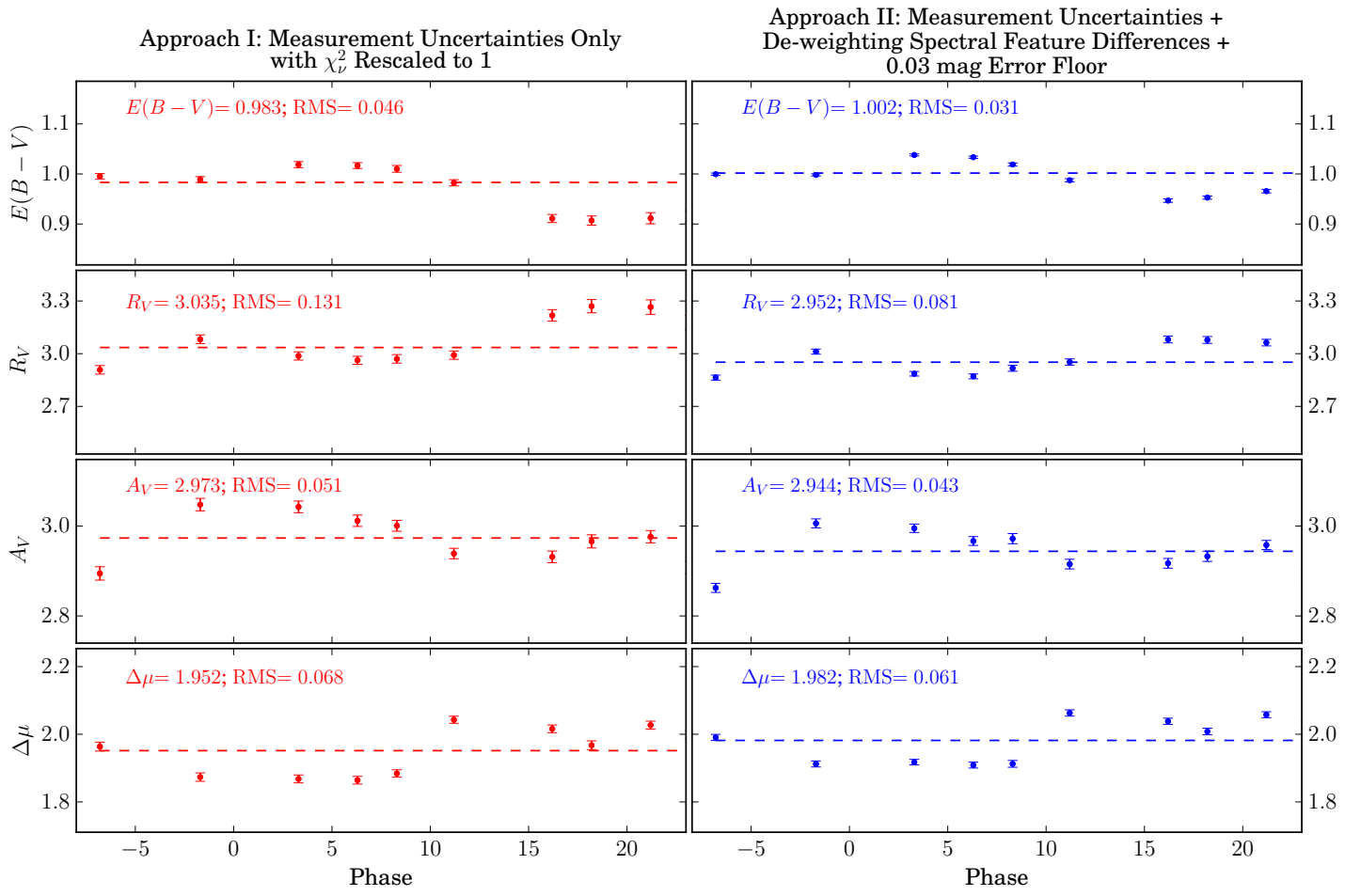

Figure 7. The best-fit R_V, $E(B-V)$, $\Delta\mu$, and the derived quantity, A_V, for the 10 phases of SN 2012cu between −6.8 and 23.2 days. The weighted averages of these quantities are drawn as dashed lines and are printed in their respective panels, along with the RMS dispersions. **Left Column**: Summary of best-fit results from Approach I, where we only take into account measurement uncertainties, but rescale to $\chi^2_\nu \sim 1$ (see text) to determine the uncertainties of the fitting parameters for each phase. **Right Column**: Summary of best-fit results from Approach II, where in addition to taking into account the measurement uncertainties, we de-weight the wavelength regions where the spectral differences are high (see text) and add a 0.03 mag error floor. The results from these two approaches differ slightly and only past day 15. Overall, Approach II more than halves the variance for R_V. The anti-correlation across the phases between R_V and $E(B-V)$ can be seen in both cases. The RMS scatters seen here (and in Tables 1 and 2) are larger than what the per-phase error bars indicate. We address this discrepancy in § 4.2.

For Approach II, the results for the last four epochs are half as far from the mean compared with

Approach I. Since late epochs are where light echoes (e.g. Patat 2005) can become most prominent, this is an important improvement.

Table 3. Comparison of Approaches I, II, and III

Spectral Mismatch Approach	$E(B-V)$		R_V		A_V		$\Delta\mu$	
	mean	RMS	mean	RMS	mean	RMS	mean	RMS
I. Not De-weighted (§3.1.1)	0.983	0.046	3.035	0.131	2.973	0.051	1.952	0.068
II. De-weighted (§3.1.2)	1.002	0.031	2.952	0.081	2.944	0.043	1.982	0.061
III. Removed (§3.1.2)	0.999	0.029	2.963	0.079	2.950	0.048	1.972	0.067

3.2. *Na I and DIB Features in SN 2012cu Spectra*

We will now examine the Na I and two DIB absorption features in the SN 2012cu spectra. All three features, Na I, DIB at 5780 Å, and DIB at 6283 Å, are at the same redshift as the H I along the sightline toward SN 2012cu in NGC 4772 (Haynes et al. 2000).

Na I Absorption: For known dust-to-gas ratio, the Na I column density can be used to infer the amount of dust along the line of sight. In addition, the correlation between extinction and the EW of Na I was first noticed decades ago (e.g. Merrill & Wilson 1938) and has been extensively studied since (e.g. Richmond et al. 1994; Turatto et al. 2003; Poznanski et al. 2012; Phillips et al. 2013). We can clearly see the Na I D feature due to the doublet $\lambda\lambda$5896, 5890 Å in the SN 2012cu spectra (Figure 8, 9). Sternberg et al. (2014) obtained high resolution measurement of the neutral Na features of SN 2012cu at four epochs.. Their spectrum at a phase of 8 days gives (EW_{D1}, EW_{D2}) = (857 ± 6 mÅ, 928 ± 6 mÅ), and shows that the lines are so saturated that the Na I column density cannot be measured accurately.

We measure EW(NaD) in our low resolution SNIFS spectra for 16 epochs, spanning phases of −6.8 to 46.2 days, for which the S/N was adequate. Our model consisted of Gaussians for the D1 and D2 components, simultaneously fit with a background parametrized by a fourth order polynomial. The width of the Gaussians are set equal to the 3.42 Å RMS of the SNIFS line spread function. The ratio of the lines was set to unity to reflect the strong saturation observed in the UVES spectrum. The SNIFS spectrum taken at the same phase as the UVES spectrum yields EW(NaD) = 1790 ± 80 mÅ in good agreement with the UVES results $EW_{D1} + EW_{D2}$ = 1785 ± 8 mÅ. For the full SNIFS spectral time series, we find a mean ⟨EW(NaD)⟩ = 1560 mÅ with RMS = 130 mÅ, with $\chi^2_\nu = 3.0$. This EW is marginally lower than the values from the UVES spectrum. But the somewhat high χ^2_ν suggests the presence of extra noise, likely due to residual structure in SN spectral features that is difficult

to completely remove from our low-resolution spectra. There is no indication of any coherent trend with phase. Because the Na D line is so strongly saturated, only variability having a velocity at the extremities of the lines could have been detected.

DIB Features: The DIBs have a well-known association with dust (e.g. Heger 1922; Merrill 1934; Herbig 1995; Cox & Patat 2008; Hobbs et al. 2008). We find many DIB features in the high resolution VLT UVES spectrum of SN 2012cu at a phase of 8 days. The DIBs at 5780 Å and 6283 Å are strong enough to be found in the SNIFS spectra (Figures 8, 9). Phillips et al. (2013) used the EW of the DIB feature at 5780 Å to measure extinction for a number of SNe Ia. We find this feature in our spectra for phases −6.8, −3.8, −1.7, 3.3, and 6.3 days (Figure 9). This feature is located in a Si II absorption line, making it challenging to fit. The approach that works best is to simultaneously fit this absorption feature and the background in a 100 Å window around 5780 Å with a Gaussian and a third order polynomial (Figure 10). The convolution of this feature, with an intrinsic FWHM of 2.11 Å (Hobbs et al. 2008; Phillips et al. 2013), and the SNIFS line-spread-function for the red channel yields a net RMS width of 3.54 Å. We thus fix the width of the Gaussian at this value. (From the UVES spectrum we also identify the weak 5800 Å DIB, of which we can see a hint in the panel for phase −3.8 days in Figure 10. At the existing S/N, it does not affect our fit.) After normalizing by the fitted the background, we find the values $\mathrm{EW_{DIB}}(5780\ \text{Å}) = 292\pm97$, 390 ± 76, 355 ± 62, 370 ± 74, and 432 ± 71 mÅ for these five phases, respectively. The weighted mean is 357 ± 34 mÅ, and there is no evidence of time variation. From the high resolution VLT UVES spectrum at 8 days we measure $\mathrm{EW_{DIB}}(5780\ \text{Å}) = 360\pm5$ mÅ, in agreement with the results from the lower resolution SNIFS spectra.

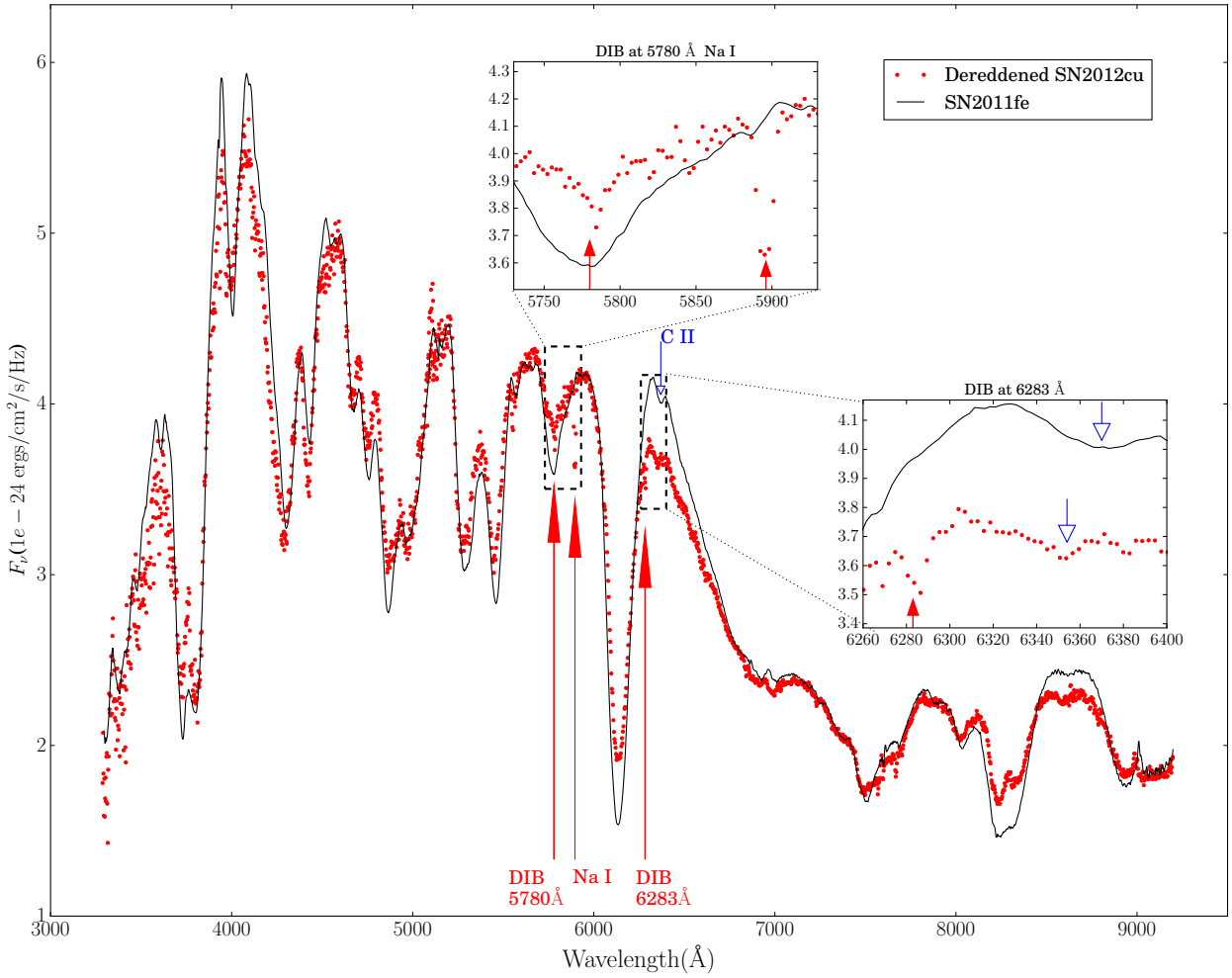

Figure 8. Na I and DIB features. The solid line (black) and the dots (red) show the spectra of SN 2011fe at −2.0 days and SN 2012cu at −1.7 days, respectively. The spectrum of SN 2012cu has been dereddened according to the best-fit $E(B-V)$ and R_V (see Figure 6 or Table 2) for this phase. Its flux has also been scaled according to the best-fit $\Delta\mu$ to correspond to the distance of SN 2011fe. The DIB absorption at 5780 Å and the Na I feature can be clearly seen (red arrows with filled arrowheads). We also indicate another known DIB feature at 6283 Å (red arrow with filled arrowhead). All three features are at the redshift of the H I toward SN2012cu in NGC 4772 (Haynes et al. 2000). The intrinsic C II λ6580 Å feature is also shown (blue arrow with unfilled arrowhead).

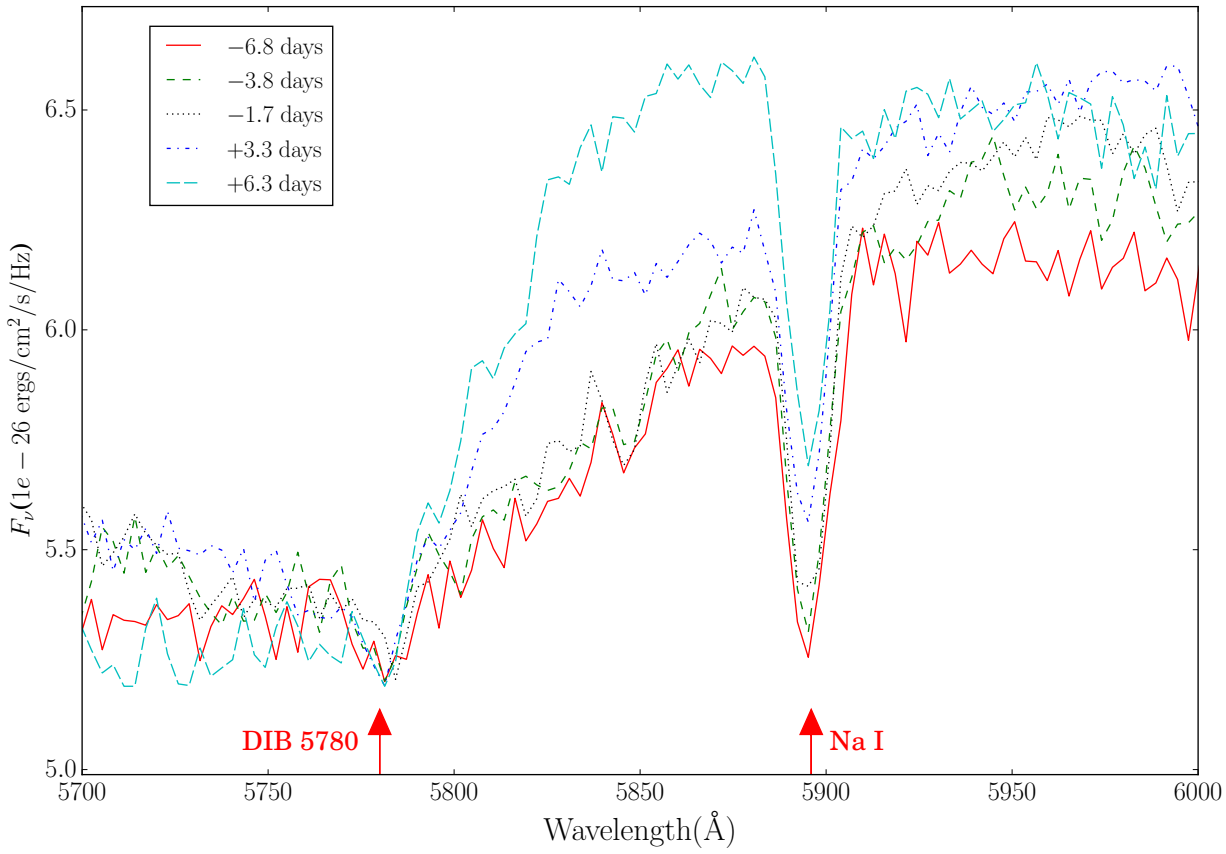

Figure 9. Zoom around key ISM features. The solid (red), dashed (green), dotted (black), dash-dotted (blue) and long-dashed (cyan) lines are SN 2012cu spectra flux-matched at the bottom of a notch near 5780 Å for the phases of −6.8, −3.8, −1.7, 3.3, and 6.3 days, respectively. The DIB absorption feature at 5780 Å, situated near the minimum of a Si II feature, can now be clearly seen. The Na I absorption feature to the right is also readily apparent.

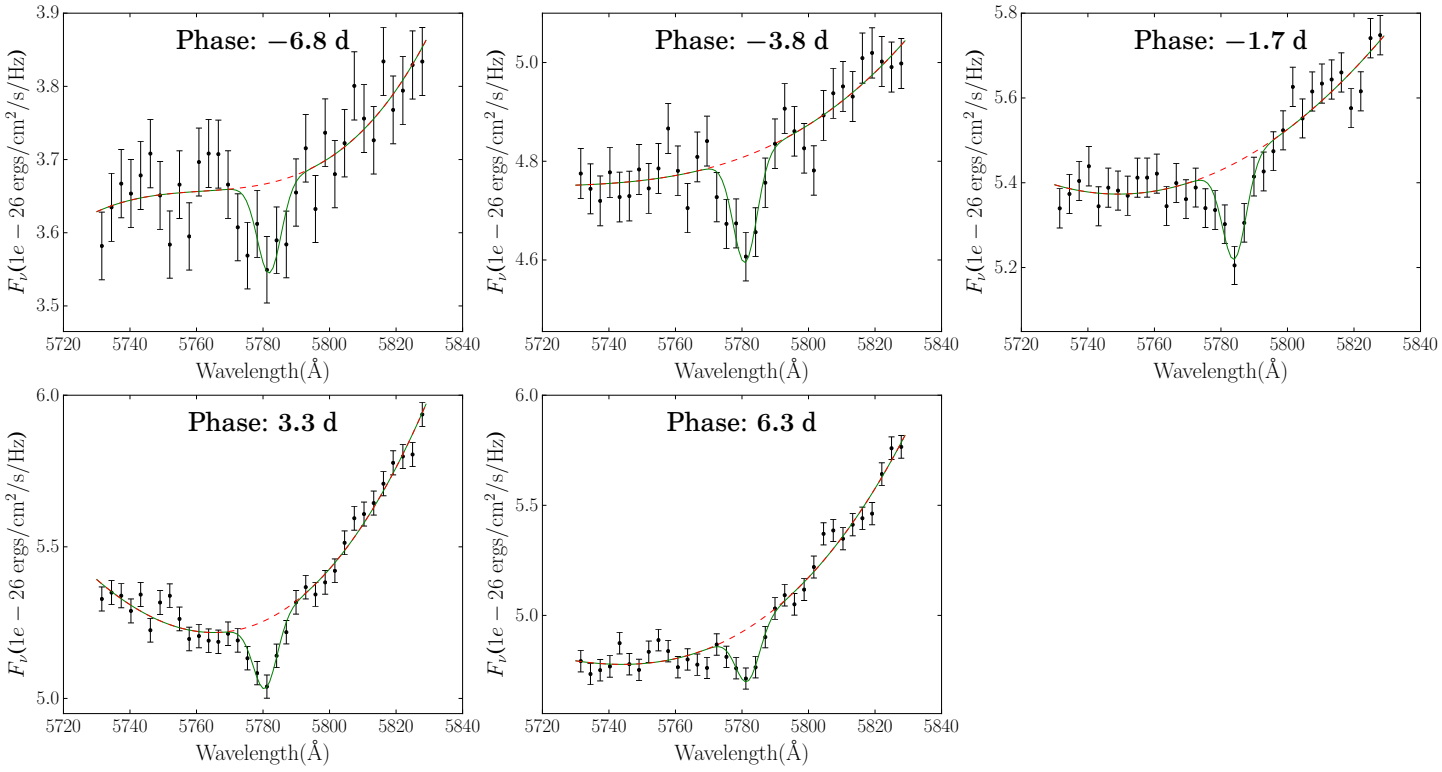

Figure 10. Zoom of the spectral region covering the DIB 5780 Å feature identified in Figure 9 for each epoch where it is well-detected. The green curve in each panel shows a simultaneous fit with a Gaussian, and a third order polynomial for the background (red dashed curve). We normalize by the background and determine the EW for each epoch. We find an average EW of 357±34 mÅ. This mean value is confirmed by our measurement of 360±5 mÅ for the EW of the same feature from a high resolution VLT UVES spectrum at a phase of 8 days. This is about $1\,\sigma$ below the MW average, 609^{+402}_{-242} mÅ, expected using our best-fit A_V found in § 3.1.2 (see Phillips et al. 2013).

4. DISCUSSION

We now discuss some of the implications of our measurements, specifically, the distance to the SN 2012cu host galaxy and the nature of the veiling dust.

4.1. *Measurement of Host Distance*

The distance modulus differences between SN 2012cu and SN 2011fe ($\Delta\mu$) from Approach I (§3.1.1), II, and III (both in §3.1.2) are in agreement with each other — to better than their respective RMS dispersions (Table 3). As presented in § 3.1.2, the average value over 10 epochs from Approach II has been adopted as the best-fit relative distance modulus: ($\Delta\mu$, RMS) = (1.982, 0.061) mag. If we combine the gray scatter for SN 2012cu and SN 2011fe mentioned in § 3.1.1, we expect an RMS across the phases to be 0.052 mag. With 10 phases, we expect the uncertainty on the RMS to be 0.013 mag. Thus it is likely that the gray scatter can fully explain the RMS of 0.061 mag for $\Delta\mu$. But it is also possible that there are additional sources of uncertainty that may not be statistical. Below we consider both possibilities.

The distance to the host galaxy of SN 2011fe, M101, has been measured most recently and accurately using the Cepheid period-luminosity relation (Shappee & Stanek 2011; Mager et al. 2013; Nataf 2015) and "tip of the red giant branch" (TRGB; Shappee & Stanek 2011; Lee & Jang 2013) techniques. Adjusting these published values to a common distance modulus of 18.477 ± 0.033 mag for the LMC (Freedman et al. 2012) gives a distance modulus to M101 of 29.114 ± 0.072 mag. The RMS scatter between the five measurements is 0.10 mag and the weighted means of the Cepheid and TRGB measurements agree within 0.04 mag. Adopting this distance to M101 with our measured $\Delta\mu$ results in a distance modulus of 31.11±0.15 mag for NGC 4772, the host of SN 2012cu. This corresponds to 16.6±1.1 Mpc. SNe Ia exhibit a random per-object scatter of ~ 0.15 mag when standardized using lightcurve width and color. However, closely matched "twin" SNe Ia like SN 2011fe and

SN 2012cu show a much smaller per-object scatter. For the twinness ranking of the pair SN 2012cu and SN 2011fe (at top 10%), the scatter is expected be 0.086 mag (Fakhouri et al. 2015). Removing the gray scatter of 0.025 mag quoted there, we obtain 0.082 mag. If we treat the RMS dispersion for $\Delta\mu$ as purely statistical, the uncertainty on $\Delta\mu$ is $\sigma_{\Delta\mu} = \sqrt{2 \cdot 0.082^2 + 0.061^2/(10-1)} = 0.12$ mag. If we take the extreme position that all of the RMS dispersion comes from non-statistical sources, then $\sigma_{\Delta\mu}$ becomes 0.13 mag. Thus for the host galaxy of SN 2012cu, after adding the uncertainty for the SN 2011fe distance, $\sigma_\mu = 0.14$ or 0.15 mag, for these two possibilities respectively.

NGC 4772 is usually considered part of the Virgo Southern Extension (Tully 1982). Using an infall model, Kim et al. (2014) concluded NGC 4772 is a member of the Virgo Cluster proper. A previous determination of its distance modulus can be found on the Extragalactic Distance Database[2] (EDD, Tully et al. 2009): 30.96 ± 0.13 mag, corresponding to 15.6±1 Mpc. This is in excellent agreement with our value. Interestingly, the specific distance to NGC 4772 quoted in Tully et al. (2008) is highly discrepant with both the EDD distance, which is the average distance for a group of 11 galaxies, to which NGC 4772 is assigned, and our value. Haynes et al. (2000) found that the stars and the ionized gas in the center of NGC 4772 are counter-rotating, which is often taken as an indication of a merger. If the bulk of the gas in NGC 4772 is from a merger, the H I line-width would likely be inflated. For the Tully-Fisher relation, this would result in a measured distance that is too large. Therefore we consider the EDD value, rather than the value from Tully et al. (2008) for this galaxy, as the most appropriate for this comparison.

If on the other hand, had we mimicked a cosmological fit, e.g., using a value of $\beta \sim 3.1$ (Betoule et al. 2014) and combining it with the SALT $c = 0.971$ for SN 2012cu, the estimated distance to NGC 4772 would have been 26 Mpc. This would place NGC 4772 well beyond the distance of the Virgo Cluster. Given the uncertainty surrounding the integrity of the H I line width for an apparent merger like NGC 4772, we advocate another independent measurement of the distance, e.g., using

the TRGB or the surface brightness fluctuation (SBF) method. If the TRGB or SBF distance also agrees with our distance measurement, that would further validate that our approach of correcting for the extinction using the twins method yields the correct distance.

4.2. *Nature of Dust*

4.2.1. *Upper Limit on Time Variability*

Figures 7 shows that the dispersions for the dust quantities, R_V, $E(B-V)$, and A_V are small. There is the suggestion of shallow trends in phase for R_V and $E(B-V)$, but in opposite directions. The trends appear stronger for Approach I (Figure 7, left column). The effects might be real, but consider the following: 1. Systematic uncertainties unrelated to dust, e.g., slightly different SN astrophysics even for good but not perfect "twins," likely remain. The (likely small) difference in their time evolution may be responsible for the these trends. The fact that when we de-weight the spectral feature differences in Approach II, the trends in $E(B-V)$ and R_V clearly become even weaker is consistent with this conjecture. 2. The remaining very shallow trends in $E(B-V)$ and R_V in Approach II (Figure 7, right column) still point in opposite directions. If there were time variation associated with dust, whether due to ISM or CSM, the first order effect would be the time variation of A_V, with $E(B-V)$ following the same trend (e.g., for ISM, see Patat et al. (2010), Förster et al. (2013); for CSM, see Wang (2005), Goobar (2008), Brown et al. (2015)). However, there is no clear trend for A_V in Figure 7. While our model does not capture what may be responsible for the very weak trends that remain in R_V and $E(B-V)$ in Approach II, their opposite directions may be related to the per-phase anti-correlation between these two quantities noted in § 3.1.1. We therefore hesitate to claim that the apparent but shallow trends in phase for R_V or $E(B-V)$ are real. At this point we regard the RMS values of the fluctuations in R_V and $E(B-V)$ as the upper limits for their

[2] http://edd.ifa.hawaii.edu/

time variation. To confirm subtler variability would require a pair of SNe even more closely twinned than SN 2011fe and SN 2012cu. Finally, while it is true that the systematic scatter is greater than the error bars from fitting (Figure 7), the spectral time series for these two SNe were measured so well that the fitting errors are far below the scale of interest scientifically. The systematic scatters themselves are small. Thus, even if these shallow trends were real, we expect the implications would be minor.

4.2.2. *Lack of Evidence for CSM Dust*

Simulations of extinction due to CSM dust carried out by Wang (2005) and Brown et al. (2015) show that for the phase range probed in this paper, $E(B-V)$ and A_V should monotonically decrease over time with a similar fractional rate, and as a result R_V would only vary slightly. Those simulated changes in A_V and $E(B-V)$ are much greater than seen in Figure 7. Changes in CSM ionization conditions due to SN ultraviolet radiation can also lead to variable EW(Na I) (Patat et al. 2007). However, there is no evidence for EW(Na I) variation in Sternberg et al. (2014) nor in our measurements of the SNIFS spectra.

4.2.3. *Evidence for ISM Dust*

The R_V value we have obtained, 2.952 ± 0.081, is very similar to MW average. The expected EW for DIB 5780 Å based on MW observations from Equation 6 of (Phillips et al. 2013) is 609^{+406}_{-242} mÅ, and the direct measurement for NGC 4772, 357 ± 34 mÅ, agree within the expected scatter. In addition, as mentioned in § 3.2, we see many other DIB features in the VLT UVES spectrum. Using the MW average relationship between EW(Na I) and $E(B-V)$ in Poznanski et al. (2012) and the total EW(Na I) from Sternberg et al. (2014), Amanullah et al. (2015) obtained an $E(B-V)$ prediction that is approximately $2\,\sigma$ higher than the measured value for SN 2012cu. To some degree this is expected given the very strong saturation of the Na I D absorption and is consistent with the larger

scatter on A_V vs. EW(Na I) found for SNe by Phillips et al. (2013).

Lending support to ISM dust being the cause of the reddening for SN 2012cu is the projected position of SN 2012cu onto a dust lane in its host galaxy (Figure 1). The disk rotation of NGC 4772 was measured by Haynes et al. (2000) who identified an inner ring of H I that is co-spatial with the dust ring. At the projected location of SN 2012cu, the H I velocity contours of their Figure 12 give a mean of 90 km/s. From the UVES spectrum, we have measured the velocities of the Na I D and DIB 5780 Å extinction tracers to be 89 km/s and 102 km/s, respectively. These values match well with the H I velocity at the location of SN 2012cu. Haynes et al. (2000) also provided the bulge-disk decomposition of stellar light, which at the location of SN 2012cu has a bulge-to-disk flux ratio of ~ 0.07, indicating that SN 2012cu is most likely in the disk of NGC 4772. Taken together, it is therefore highly likely that SN 2012cu is embedded in or behind the ISM dust lane.

In summary, we find that the observational evidence strongly suggests that the dominant, if not all, foreground dust component in the host of SN 2012cu is interstellar in nature and is similar to MW dust.

An interesting new avenue for constraining R_V, independent of SN Ia colors and astrophysics, is the correlation between the apparent dust emissivity power law index, β_{FIR}, and R_V, found for Milky Way sightlines by Schlafly et al. (2016). It so happens that NGC 4772 was observed in the thermal IR using *Herschel*, yielding $\beta_{FIR} = 2.1 \pm 0.3$ (Cortese et al. 2014). While typical for many galaxies, this is outside the range spanned by the MW Schlafly et al. (2016) data. But if a linear extrapolation is applicable, it would predict $R_V(\beta_{FIR}) = 2.2 \pm 0.7$. This is lower than, but consistent with our measurement based on twin SN Ia optical spectra. β_{FIR} has well-established correlations with galaxy metallicity, gas mass fraction, and stellar mass surface density (Cortese et al. 2014). Unless these differences translate directly into differences in R_V — a situation that would be relevant for extinction correction of SNe Ia — then differences between the properties of the NGC 4772 dust ring and the

Milky Way dust could bias this method. The size of the uncertainty further illustrates that it may prove challenging to measure β_{FIR} with sufficient accuracy to help resolve the tension between the cosmologically-derived β and SN-color based measurements of R_V.

It is worth noting that there is at least one other SN Ia with high extinction and a MW-like R_V, SN 1986G, with $A_V \sim 2.0$ and $R_V = 2.57^{+0.23}_{-0.21}$ (Phillips et al. 2013) based on optical and NIR photometry[3]. An earlier R_V value of 2.4 for SN 1986G was reported by Hough et al. (1987) based on polarimetry and the Serkowski relation between peak polarization wavelength and R_V (Serkowski et al. 1975). Even though SN 1986G is considered a weak and peculiar event (Phillips et al. 1987; Branch 1998), the host galaxies for SN 1986G and SN 2012cu, NGC 5128 and NGC 4772, respectively, are both large, mostly passive galaxies with a "frosting" of young stars and dust lanes indicative of a merger (for a review on NGC 5128, see Israel 1998; for NGC 4772, see Haynes et al. 2000). Like SN 2012cu, SN 1986G is projected onto its host galaxy dust lane and the dust lane is considered to be the source of its reddening (Phillips et al. 1987, 2013).

5. CONCLUSIONS

We have used a high-quality spectrophometric time series obtained by the SNfactory to study the highly reddened Type Ia SN 2012cu. We analyzed 10 phases between −6.8 and 23.2 days, using the phase-matched spectra of SN 2011fe as an unreddened template. By simultaneously fitting for $E(B-V)$, R_V, and $\Delta\mu$, the distance modulus difference between the two SNe, we have found that SN 2012cu is highly reddened, with ($E(B-V)$, RMS) = $(1.002, 0.031)$, (R_V, RMS) = $(2.952, 0.081)$, (A_V, RMS) = $(2.944, 0.043)$, and ($\Delta\mu$, RMS) = $(1.982, 0.061)$. Our best-fit $E(B-V)$ agrees well with the corresponding value reported in Amanullah et al. (2015) for SN 2012cu based on broadband

[3] Even though Phillips et al. (2013) used the extinction curve of CCM89, their R_V value for SN 1986G might not be severely underestimated due to their inclusion of a larger wavelength coverage and the dilution of the 5500 – 8900 Å region by the addition of NIR photometry (see Appendix A).

photometry from UV to NIR, and our best-fit R_V is slightly higher than theirs.

Spectral Diversity and Relative Distance Measurement with Supernova Twins. We find that SN 2012cu and SN 2011fe are excellent spectroscopic twins according to the method of Fakhouri et al. (2015). We have treated the modest spectral differences that remain in different ways. The consistency of our measurement of A_V and $\Delta\mu$ between these approaches demonstrates that despite the presence of spectral feature differences, spectroscopically twinned SNe can be used to accurately measure relative distances, in this case between M101 and NGC 4772, the host galaxies to the two SNe, to 6.0%.

Host Distance. We measure the distance modulus to the host galaxy of SN 2012cu, NGC 4772, to be 31.10 ± 0.15 mag, corresponding to a distance of 16.6±1.1 Mpc. Our result is in excellent agreement with the value found on EDD.

Nature of Dust Toward SN 2012cu. While it is difficult to completely eliminate a contribution from circumstellar dust, together the following factors strongly suggest that the dominant dust component along the line of sight to SN 2012cu is interstellar in nature and is similar to MW dust:

1) it's highly likely that SN 2012cu is embedded in or behind its host-galaxy dust lane;

2) the agreement between our best-fit R_V and the MW average value;

3) the lack of time variation in $E(B-V)$ and A_V;

4) the lack of time varying Na I (or DIB 5780 Å) absorption;

5) our measurement of the 5780 Å DIB and A_V agree with the average MW relation;

6) the presence of many other DIB features identified in the high resolution VLT UVES spectrum;

7) our measurement of Na I absorption and A_V agree with the broad trend seen in the MW.

6. ACKNOWLEDGEMENT

We thank the technical staff of the University of Hawaii 2.2 m telescope, and Dan Birchall for observing assistance. We recognize the significant cultural role of Mauna Kea within the indigenous Hawaiian community, and we appreciate the opportunity to conduct observations from this revered site. This work was supported in part by the Director, Office of Science, Office of High Energy Physics of the U.S. Department of Energy under Contract No. DE-AC02- 05CH11231. We thank the Gordon & Betty Moore Foundation for their continuing support. XH acknowledges the University of San Francisco (USF) Faculty Development Fund. ZR was supported in part by a USF Summer Undergraduate Research Fellowship. Support in France was provided by CNRS/IN2P3, CNRS/INSU, and PNC; LPNHE acknowledges support from LABEX ILP, supported by French state funds managed by the ANR within the Investissements d'Avenir programme under reference ANR-11-IDEX-0004-02. NC is grateful to the LABEX Lyon Institute of Origins (ANR-10-LABX-0066) of the Université de Lyon for its financial support within the program "Investissements d'Avenir" (ANR-11-IDEX-0007) of the French government operated by the National Research Agency (ANR). Support in Germany was provided by the DFG through TRR33 "The Dark Universe;" and in China from Tsinghua University 985 grant and NSFC grant No 11173017. This works is partially based on observations made with ESO Telescopes at the La Silla Paranal Observatory, Chile, under program 289.D-5035. Some results were obtained using resources and support from the National Energy Research Scientific Computing Center, supported by the Director, Office of Science, Office of Advanced Scientific Computing Research of the U.S. Department of Energy under Contract No. DE-AC02- 05CH11231.

REFERENCES

Aldering, G., Adam, G., Antilogus, P., et al. 2002, in Society of Photo-Optical Instrumentation Engineers (SPIE) Conference Series, Vol. 4836, Survey and Other Telescope Technologies and Discoveries, ed. J. A. Tyson & S. Wolff, 61–72

Aldering, G., Antilogus, P., Bailey, S., et al. 2006, ApJ, 650, 510

Amanullah, R., Goobar, A., Johansson, J., et al. 2014, ApJL, 788, L21

Amanullah, R., Johansson, J., Goobar, A., et al. 2015, MNRAS, 453, 3300
Bacon, R., Adam, G., Baranne, A., et al. 1995, A&AS, 113, 347
Bacon, R., Copin, Y., Monnet, G., et al. 2001, MNRAS, 326, 23
Barone-Nugent, R. L., Lidman, C., Wyithe, J. S. B., et al. 2012, MNRAS, 425, 1007
Berry, M., Ivezić, Ž., Sesar, B., et al. 2012, ApJ, 757, 166
Bessell, M., & Murphy, S. 2012, PASP, 124, 140
Betoule, M., Kessler, R., Guy, J., et al. 2014, A&A, 568, A22
Bianchi, L., Conti, A., & Shiao, B. 2014, VizieR Online Data Catalog, 2335
Bongard, S., Soulez, F., Thiébaut, É., & Pecontal, É. 2011, MNRAS, 418, 258
Branch, D. 1998, ARA&A, 36, 17
Brown, P. J., Smitka, M. T., Wang, L., et al. 2015, ApJ, 805, 74
Buton, C., Copin, Y., Aldering, G., et al. 2013, A&A, 549, A8
Cardelli, J. A., Clayton, G. C., & Mathis, J. S. 1989, ApJ, 345, 245
Chotard, N., Gangler, E., Aldering, G., et al. 2011, A&A, 529, L4
Cortese, L., Fritz, J., Bianchi, S., et al. 2014, MNRAS, 440, 942
Cox, N. L. J., & Patat, F. 2008, A&A, 485, L9
de Vaucouleurs, G., de Vaucouleurs, A., Corwin, Jr., H. G., et al. 1991, Third Reference Catalogue of Bright Galaxies. Volume I: Explanations and references. Volume II: Data for galaxies between 0^h and 12^h. Volume III: Data for galaxies between 12^h and 24^h.
Draine, B. T. 2003, ARA&A, 41, 241
Fakhouri, H. K., Boone, K., Aldering, G., et al. 2015, ApJ, 815, 58
Fitzpatrick, E. L. 1999, PASP, 111, 63
Foley, R. J., & Kasen, D. 2011, ApJ, 729, 55
Foley, R. J., Fox, O. D., McCully, C., et al. 2014, MNRAS, 443, 2887
Förster, F., González-Gaitán, S., Folatelli, G., & Morrell, N. 2013, ApJ, 772, 19
Freedman, W. L., Madore, B. F., Scowcroft, V., et al. 2012, ApJ, 758, 24
Ganeshalingam, M., Cenko, S. B., Li, W., et al. 2012, Central Bureau Electronic Telegrams, 3154, 1
Goobar, A. 2008, ApJL, 686, L103
Goobar, A., Johansson, J., Amanullah, R., et al. 2014, ApJL, 784, L12
Guy, J., Astier, P., Baumont, S., et al. 2007, A&A, 466, 11
Guy, J., Sullivan, M., Conley, A., et al. 2010, A&A, 523, A7
Haynes, M. P., Jore, K. P., Barrett, E. A., Broeils, A. H., & Murray, B. M. 2000, AJ, 120, 703
Heger, M. L. 1922, Lick Observatory Bulletin, 10, 141
Herbig, G. H. 1995, ARA&A, 33, 19
Hicken, M., Wood-Vasey, W. M., Blondin, S., et al. 2009, ApJ, 700, 1097
Hobbs, L. M., York, D. G., Snow, T. P., et al. 2008, The Astrophysical Journal, 680, 1256
Hough, J. H., Bailey, J. A., Rouse, M. F., & Whittet, D. C. B. 1987, MNRAS, 227, 1P
Israel, F. P. 1998, A&A Rv, 8, 237
Itagaki, K., Howerton, S., Noguchi, T., et al. 2012, Central Bureau Electronic Telegrams, 3146, 1
Kelly, P. L., Filippenko, A. V., Burke, D. L., et al. 2015, Science, 347, 1459
Kim, S., Rey, S.-C., Jerjen, H., et al. 2014, ApJS, 215, 22
Lantz, B., Aldering, G., Antilogus, P., et al. 2004, in Society of Photo-Optical Instrumentation Engineers (SPIE) Conference Series, Vol. 5249, Optical Design and Engineering, ed. L. Mazuray, P. J. Rogers, & R. Wartmann, 146–155
Lee, M. G., & Jang, I. S. 2013, ApJ, 773, 13
Li, A., & Draine, B. T. 2001, ApJ, 554, 778
Mager, V. A., Madore, B. F., & Freedman, W. L. 2013, ApJ, 777, 79
Mandel, K. S., Narayan, G., & Kirshner, R. P. 2011, ApJ, 731, 120
Marion, G. H., Milisavljevic, D., Rines, K., & Wilhelmy, S. 2012, Central Bureau Electronic Telegrams, 3146, 2
Marion, G. H., Sand, D. J., Hsiao, E. Y., et al. 2015, ApJ, 798, 39
Merrill, P. W. 1934, PASP, 46, 206
Merrill, P. W., & Wilson, O. C. 1938, ApJ, 87, 9
Mörtsell, E. 2013, A&A, 550, A80
Nataf, D. M. 2015, MNRAS, 449, 1171
Nugent, P. E., Sullivan, M., Cenko, S. B., et al. 2011, Nature, 480, 344
O'Donnell, J. E. 1994, ApJ, 422, 158
Patat, F. 2005, MNRAS, 357, 1161
Patat, F., Cox, N. L. J., Parrent, J., & Branch, D. 2010, A&A, 514, A78
Patat, F., Chandra, P., Chevalier, R., et al. 2007, Science, 317, 924
Pereira, R., Thomas, R. C., Aldering, G., et al. 2013, A&A, 554, A27
Perlmutter, S., Aldering, G., Goldhaber, G., et al. 1999, ApJ, 517, 565
Phillips, M. M., Phillips, A. C., Heathcote, S. R., et al. 1987, PASP, 99, 592
Phillips, M. M., Simon, J. D., Morrell, N., et al. 2013, ApJ, 779, 38
Poznanski, D., Prochaska, J. X., & Bloom, J. S. 2012, MNRAS, 426, 1465
Rest, A., Scolnic, D., Foley, R. J., et al. 2014, ApJ, 795, 44
Richmond, M. W., Treffers, R. R., Filippenko, A. V., et al. 1994, AJ, 107, 1022
Riess, A. G., Filippenko, A. V., Challis, P., et al. 1998, AJ, 116, 1009
Rigault, M., Copin, Y., Aldering, G., et al. 2013, A&A, 560, A66
Scalzo, R. A., Aldering, G., Antilogus, P., et al. 2010, ApJ, 713, 1073
Schlafly, E. F., & Finkbeiner, D. P. 2011, ApJ, 737, 103
Schlafly, E. F., Finkbeiner, D. P., Schlegel, D. J., et al. 2010, ApJ, 725, 1175
Schlafly, E. F., Meisner, A. M., Stutz, A. M., et al. 2016, ApJ, 821, 78
Serkowski, K., Mathewson, D. S., & Ford, V. L. 1975, ApJ, 196, 261
Shappee, B. J., & Stanek, K. Z. 2011, ApJ, 733, 124

Sternberg, A., Gal-Yam, A., Simon, J. D., et al. 2014, MNRAS, 443, 1849
Suzuki, N., Rubin, D., Lidman, C., et al. 2012, ApJ, 746, 85
Thomas, R. C., Aldering, G., Antilogus, P., et al. 2011, ApJ, 743, 27
Tripp, R. 1998, A&A, 331, 815
Tripp, R., & Branch, D. 1999, ApJ, 525, 209
Tully, R. B. 1982, ApJ, 257, 389
Tully, R. B., Rizzi, L., Shaya, E. J., et al. 2009, AJ, 138, 323
Tully, R. B., Shaya, E. J., Karachentsev, I. D., et al. 2008, ApJ, 676, 184
Turatto, M., Benetti, S., & Cappellaro, E. 2003, in From Twilight to Highlight: The Physics of Supernovae, ed. W. Hillebrandt & B. Leibundgut, 200
Wang, L. 2005, ApJL, 635, L33
Wang, X., Filippenko, A. V., Ganeshalingam, M., et al. 2009, ApJL, 699, L139
Wright, E. L., Eisenhardt, P. R. M., Mainzer, A. K., et al. 2010, AJ, 140, 1868
Zhang, T.-M., Lin, M.-Y., & Wang, X.-F. 2012, Central Bureau Electronic Telegrams, 3146, 3

APPENDIX

A. COMPARISON OF THREE EXTINCTION CURVE MODELS

Here we compare the extinction curve models of CCM89, OD94, and F99 for our application. We choose the SN 2012cu phase of 11.2 days (pair #6 in Table 1), for which the spectral features of SN 2011fe and SN 2012cu are the most similar. Examination of several phases indicates that the conclusions presented below are independent of the phase chosen. To provide an initial assessment of these issues, we first use the best-fit $E(B-V)$, R_V, and $\Delta\mu$ found for F99 in § 3.1.1 to deredden SN 2012cu with each of these three extinction curves and compare to the SN 2011fe spectrum at 11.0 days. We present the results in Figure A1. For OD94 and CCM89, while the fits are virtually indistinguishable from F99 for wavelengths blue-ward of 5200 Å, there clearly is tension for these two curves with the data in the wavelength region of 5500 – 8900 Å. This region roughly corresponds to the r and i bands, and the tension between extinction curves here was first pointed out by F99. For MW sight lines, when $R_V = 3.1$ is used for CCM89 and F99, they show that CCM89 overcorrects in the wavelength range that corresponds to r and i bands (their Figure 6).

Figure A2 shows that this problem with CCM89 and OD94 persists even when $E(B-V)$, R_V, and $\Delta\mu$ are optimized for each extinction curve model individually. For this comparison we used Approach I from §3.1.1, where only measurement uncertainties are taken into account, since the de-weighting in Approach II has the potential to suppress regions that differ due to the extinction curve rather than SN features. In this case, the best-fit R_V values are (CCM89, OD94, F99) = (2.23, 2.43, 2.99), with corresponding χ^2_ν = (27, 28, 20). While OD94 and CCM89 now match the data more closely in the wavelength region of 5500 – 8900 Å, clearly their agreement remains inferior to F99. Furthermore, for OD94 and CCM89 the fit in the range 5000 – 5500 Å has worsened in a systematic way. That the R_V values for CCM89 and OD94 are now lower is not a surprise: given the tension

seen in Figure A1, CCM89 and OD94 need to be "steeper" to fit the the wavelength range of 5500 – 8900 Å better, which translates to a lower best-fit R_V.

In both comparison approaches, F99 clearly provides the best fit, and OD94 the worst. This finding is in agreement with Schlafly et al. (2010), who compared the predictions of the same three extinction curve models with the colors of stars from the Sloan Digital Sky Survey (SDSS) and found that F99 fit the data the best, and OD94 the poorest. The extinction curves of OD94 and, to a lesser extent, of CCM89, were disfavored because they under-predicted the difference between the $r - i$ and $i - z$ colors (see Figure 18 of Schlafly et al. (2010)). These correspond to the same wavelength regions where we have found tension for OD94 and CCM89. Berry et al. (2012) compared the predictions of the same three extinction curves with stellar photometry from SDSS, and they also found OD94 to be inconsistent with data, although they considered CCM89 to be acceptable.

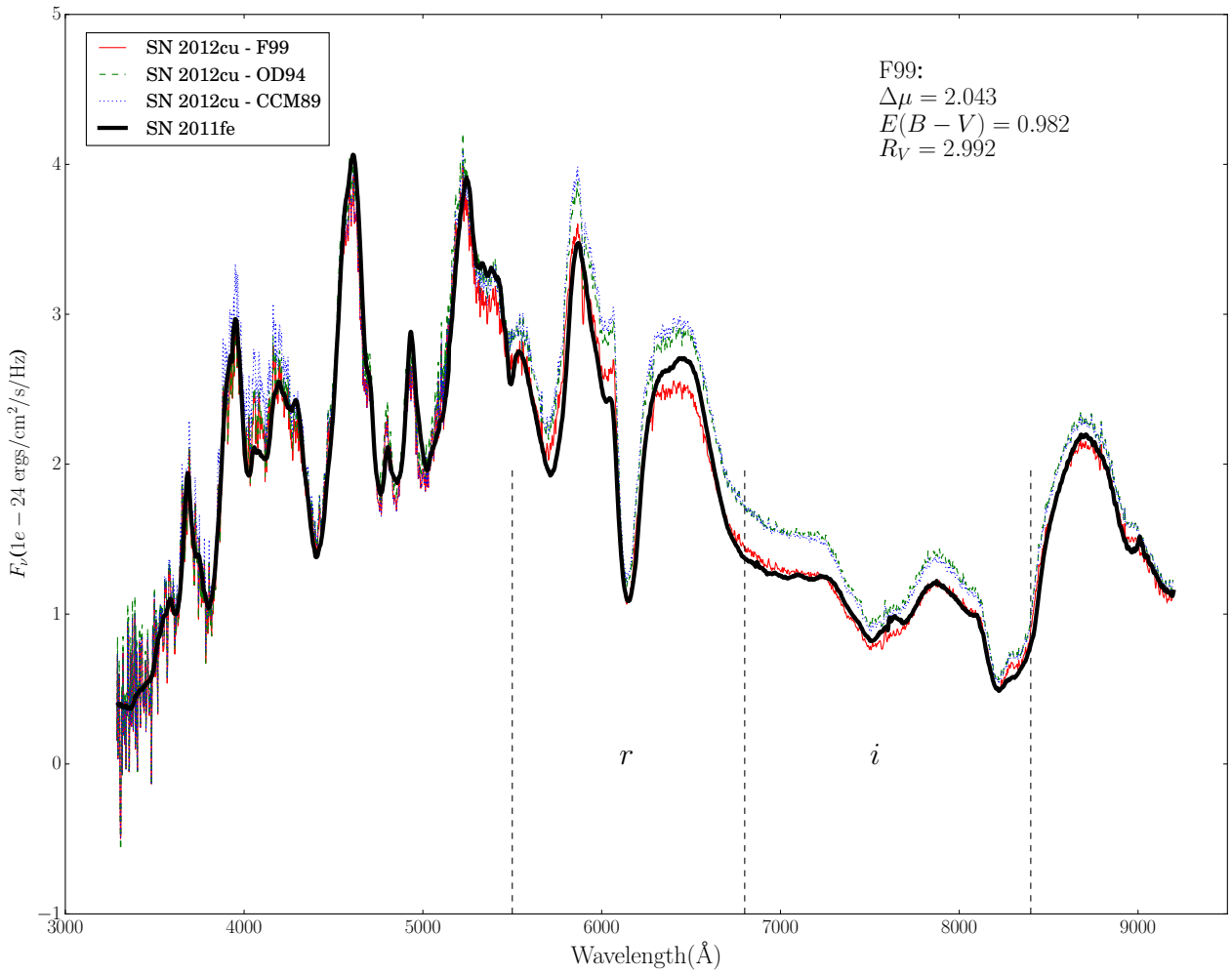

Figure A1. Using the best-fit $E(B-V)$, R_V, and $\Delta\mu$ for the F99 extinction curve model by Approach I in § 3.1.1 (see Table 2), the spectrum of SN 2012cu at 11.2 days is dereddened with the F99 (red line), OD94 (green dashed line), and CCM89 extinction curve models (blue dotted line), and then adjusted by $\Delta\mu$ to match the brightness of SN 2011fe. Also plotted is the spectrum of SN 2011fe at 11.0 days (thick black line), used as the template. The vertical dashed lines demarcate, roughly, the boundaries of the r and i filters.

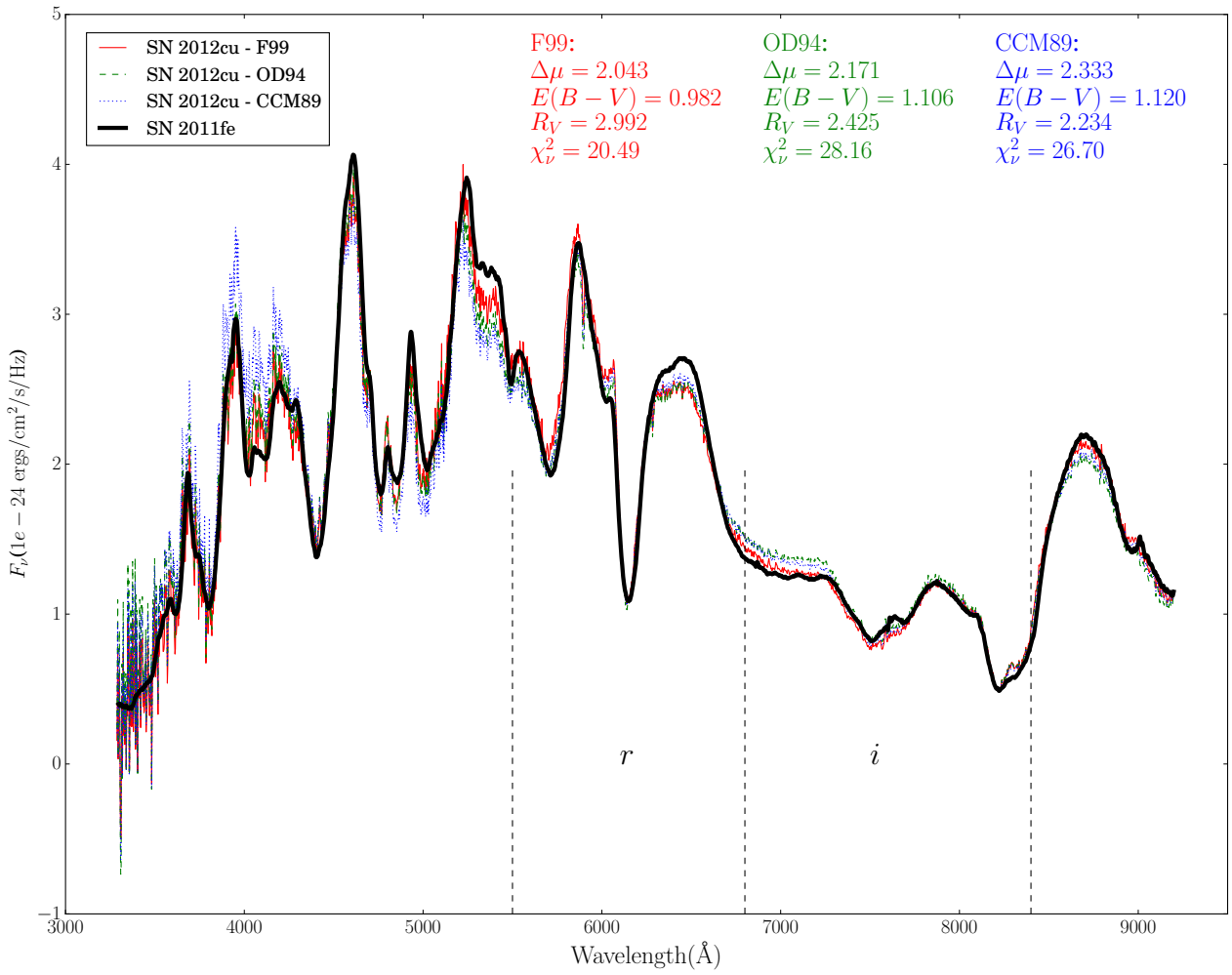

Figure A2. Comparison of the best-fit $E(B-V)$, R_V, and $\Delta\mu$ found for each of the three extinction curve models, using Approach I in §3.1.1. The spectrum of SN 2012cu at 11.2 days is dereddened with F99 (red line), OD94 (green dashed line), and CCM89 (blue dotted line), adjusted according to $\Delta\mu$ to match the brightness of SN 2011fe. Also plotted is the spectrum of SN 2011fe at 11.0 days (thick black line), used as the template. The vertical dashed lines indicate the boundaries of the r and i filters.

In addition, using extragalactic sources to constrain the MW dust properties, Mörtsell (2013) compared F99 and CCM89. Though their analysis was based on colors, it is similar to ours in the sense that both $E(B-V)$ and R_V were allowed to vary. They found that the R_V values for CCM89 were consistently lower than those for F99. For QSO's, brightest central galaxies, and

luminous red galaxies, the R_V values were (CCM89, F99) = (3.10 ± 0.43, 3.25 ± 0.37), (2.89 ± 0.88, 3.42 ± 0.48), and (1.95 ± 0.35, 3.16 ± 0.36), respectively, where the uncertainties correspond to their 95.4% confidence level. Our results, as presented in Figure A2, show the same pattern. They also made a direct comparison between the extinction values of CCM89 and F99 for the same R_V. From their Figure 13, it is clear that for $R_V = 3$, the extinction correction (A_λ) is less for F99 than for CCM89 in the wavelength region of the r and i bands. This is exactly as F99 pointed out and as we have shown in our Figure A1.

Amanullah et al. (2015) reported that for SN 2012cu their best-fit R_V for F99 (2.8 ± 0.1) and OD94 (2.8 ± 0.2) are in agreement. This may be due to the fact that the wavelength coverage in their analysis was from UV to NIR. The wide wavelength coverage may have diluted the discrepancy in the wavelength range between 5500 Å – 8900Å. However, the uncertainty for their OD94 best-fit R_V is twice as large as that for F99. We suspect that the larger uncertainty, and higher χ^2_ν, are due to the discrepancy between extinction curve models in the r and i wavelength range.

B. SN 2012CU SPECTRAL TIME SERIES DATA

Observations of SN 2012cu were obtained by the SNfactory with its SuperNova Integral Field Spectrograph (SNIFS). SNIFS is a fully integrated instrument optimized for automated observation of point sources on a structured background over the full ground-based optical window at moderate spectral resolution. It consists of a high-throughput wide-band pure-lenslet integral field spectrograph (IFS; Bacon et al. 1995, 2001), a parallel photometric channel to image the stars in the vicinity of the IFS field-of-view to monitor atmospheric transmission during spectroscopic exposures, and an acquisition/guiding channel. The IFS possesses a fully-filled $6.4'' \times 6.4''$ spectroscopic field of view subdivided into a grid of $15'' \times 15''$ spatial elements, a dual-channel spectrograph covering 3200–5200 Å and 5100–10000 Å simultaneously, and an internal calibration unit (continuum and arc lamps). SNIFS is continuously mounted on the south bent Cassegrain port of the University of Hawaii 2.2 m telescope on Mauna Kea. The telescope and instrument, under script control, are operated remotely.

SNfactory follow-up observations of SN 2012cu commenced on 2012, June 20.3, and span 53 nights. The observing log is presented in Table B1. The nominal observational cadence of 2 – 3 nights was maintained until 31.4 days after maximum brightness. The SN was observed for two more nights. The last spectra reported here were obtained 2012, Aug. 12.3. All spectra were reduced using SNfactory's dedicated data reduction pipeline (Bacon et al. 2001; Aldering et al. 2006; Scalzo et al. 2010). For non-photometric nights, we correct for clouds using field stars in the SNIFS parallel imaging camera. Detailed discussions of the flux calibration and host-galaxy subtraction are provided in Buton et al. (2013) and Bongard et al. (2011), respectively. The final spectrophotometric time series of SN 2012cu in the observer's frame is displayed in Figure B1. A tar file containing these spectra is available at http://snfactory.lbl.gov/TBD.

Table B1. Observation Log

Phase (days)	UTC Date	MJD	Photometric	Standard Stars[a]	Exp. Time(s)	Airmass	Seeing($''$)
−6.8	2012 Jun. 20.3	56098.3	N	14	820.0	1.26	0.81
−3.8	2012 Jun. 23.3	56101.3	Y	10	920.0	1.16	1.00
−1.7	2012 Jun. 25.4	56103.4	Y	11	1620.0	1.81	1.82
3.3	2012 Jun. 30.3	56108.3	Y	12	2440.0	1.65	1.65
6.3	2012 Jul. 3.3	56111.3	Y	8	1220.0	1.62	1.03
8.3	2012 Jul. 5.3	56113.3	Y	13	920.0	1.64	1.95
11.2	2012 Jul. 8.3	56116.3	Y	19	1020.0	1.44	2.06
14.2	2012 Jul. 11.3	56119.3	N	12	1020.0	1.53	1.09
16.2	2012 Jul. 13.3	56121.3	N	10	920.0	1.69	1.31
18.2	2012 Jul. 15.3	56123.3	Y	10	1520.0	1.74	1.27
21.2	2012 Jul. 18.3	56126.3	Y	11	2740.0	1.66	2.16
23.2	2012 Jul. 20.3	56128.3	Y	8	920.0	1.76	1.31
26.2	2012 Jul. 23.3	56131.3	N	13	1520.0	1.62	1.31
28.2	2012 Jul. 25.3	56133.3	Y	11	320.0	1.50	1.17
31.2	2012 Jul. 28.3	56136.3	Y	5	1220.0	1.75	1.23
41.2	2012 Aug. 7.3	56146.3	Y	9	820.0	2.07	1.37
46.2	2012 Aug. 12.3	56151.3	Y	12	820.0	2.33	1.46

[a] Number of standard stars observed during the night and used for atmospheric extinction and telluric absorption correction.

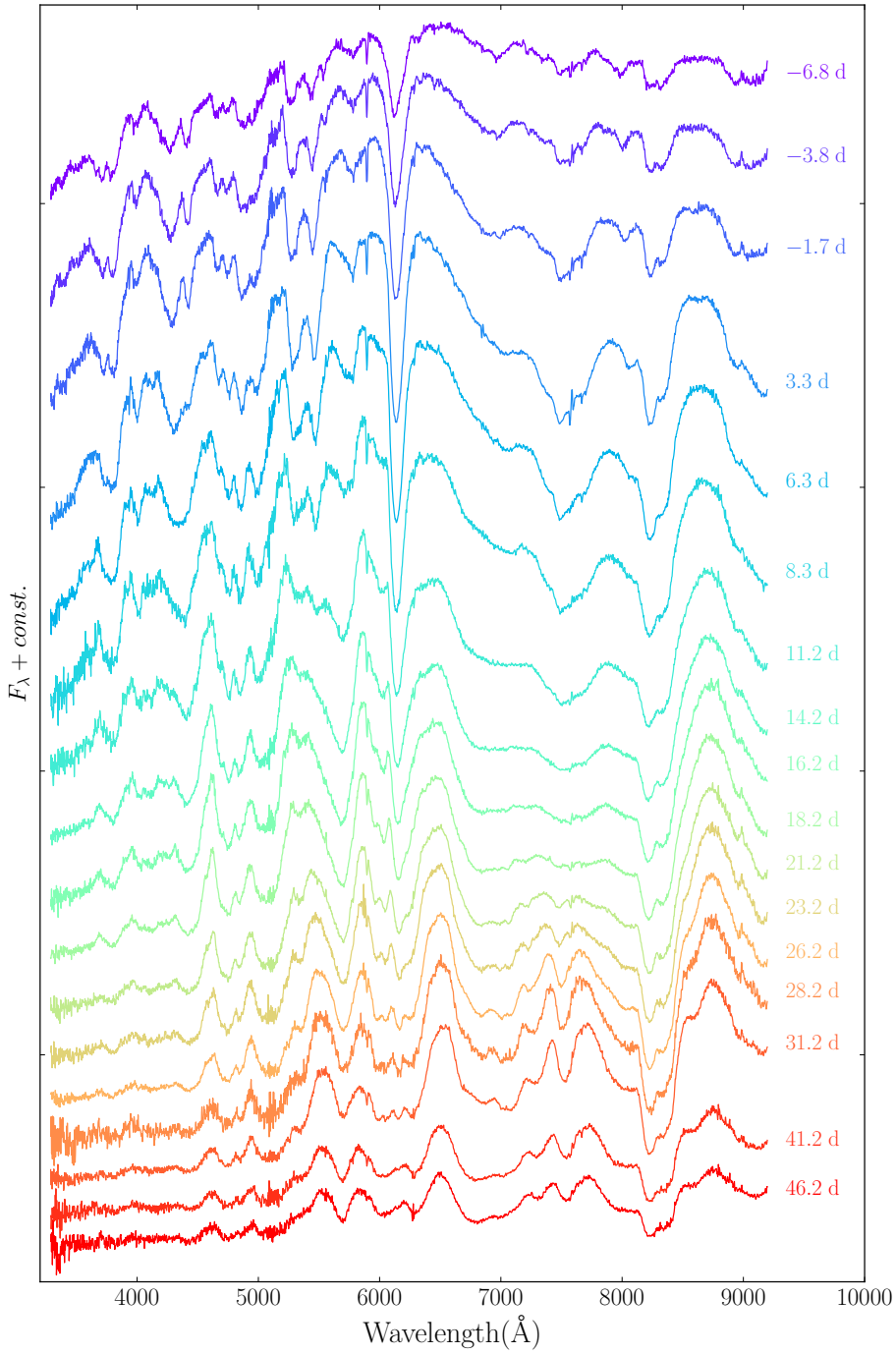

Figure B1. SNIFS spectrophotometric time series of SN 2012cu for phases of −6.8 to 46.2 days.